

Article

The Corrosion Inhibition Performance of Eco-Friendly *bis*-Schiff Bases on Carbon Steel in a Hydrochloric Solution

Arthur Valbon¹, Neubi F. Xavier, Jr.^{1,2} , Mariana F. L. P. Carlos¹ , Glauco F. Bauerfeldt¹,
Francisco W. Q. Almeida-Neto³ , Pedro de Lima-Neto³, Marcelo A. Neves⁴, Cláudio E. Rodrigues-Santos¹
and Aurea Echevarria^{1,*}

- ¹ Institute of Chemistry, Federal Rural University of Rio de Janeiro, Seropédica 23890-000, RJ, Brazil
² School of Chemistry and Chemical Engineering, University of Surrey, Guildford, Surrey GU2 7XH, UK
³ Department of Analytic Chemistry and Physical-Chemistry, Center of Sciences, Federal University of Ceará, Campus of Pici, Fortaleza 60440-900, CE, Brazil
⁴ Institute of Physics, Federal Rural University of Rio de Janeiro, Seropédica 23890-000, RJ, Brazil
* Correspondence: echevarria@ufrj.br

Abstract: Corrosion inhibitors are widely used as an important tool for the prevention and remediation of different materials exposed to corrosive industrial processes. Corrosion inhibitors are usually added to acid pickling solutions to reduce the deterioration of metallic materials and particularly, corrosion due to hydrochloric acid. In this work, three *bis*-Schiff bases (BS2, BS4 and BS8) were synthesized and characterized using spectroscopic methods, and their anti-corrosive effects on AISI 1020 carbon steel in a hydrochloric acid solution were studied using gravimetric and electrochemical techniques and quantum chemical methods. The results showed that all substances act as potential corrosion inhibitors as BS8 exhibited the highest efficiency (98%) of all methods. The compounds adsorbed on the metal surface were as per the El-Awady adsorption isotherm. Morphological aspects of the metal were observed upon applying SEM, and the theoretical results acquired from the quantum chemical calculation for molecular properties and the Fe(110) surface adsorption proved to be compatible with the experimental results.

Keywords: carbon steel; corrosion inhibitors; electrochemical methods; acidic corrosion; theoretical calculations



Citation: Valbon, A.; Xavier, N.F., Jr.; Carlos, M.F.L.P.; Bauerfeldt, G.F.; Almeida-Neto, F.W.Q.; de Lima-Neto, P.; Neves, M.A.; Rodrigues-Santos, C.E.; Echevarria, A. The Corrosion Inhibition Performance of Eco-Friendly *bis*-Schiff Bases on Carbon Steel in a Hydrochloric Solution. *Surfaces* **2023**, *6*, 509–532. <https://doi.org/10.3390/surfaces6040034>

Academic Editor: Roberto Giovanardi

Received: 17 October 2023
Revised: 10 November 2023
Accepted: 27 November 2023
Published: 6 December 2023



Copyright: © 2023 by the authors. Licensee MDPI, Basel, Switzerland. This article is an open access article distributed under the terms and conditions of the Creative Commons Attribution (CC BY) license (<https://creativecommons.org/licenses/by/4.0/>).

1. Introduction

Corrosion inhibitors are widely used as an important tool for the prevention and remediation of different materials exposed to corrosive industrial processes, such as acid pickling, and especially carbon steel, which is generally used in industries due its low cost, high strength and cost efficiency [1,2]. Corrosion inhibitors are usually added to acid pickling solutions to reduce the deterioration of metallic materials and especially corrosion due to hydrochloric acid, which is the most used since it produces cleaner and brighter surfaces, it does not require heating and its residues are more easily removed with water than sulfuric acid residue [3].

The employment of organic inhibitors in the prevention of acid corrosion is common. Thus, organic compounds that have atoms with lone pairs of electrons (nitrogen, oxygen, sulfur and phosphorous), unsaturated bonds and aromatic rings show good efficiency as corrosion inhibitor agents for carbon steel [4,5].

Schiff bases are compounds containing the chemical bond $-C=N-$ that can complex with different metals and show spontaneous monolayer formation on metal surfaces. Such properties make these compounds good candidates for being corrosion inhibitors [6,7]. Indeed, it has been shown that Schiff bases are good corrosion inhibitors presenting high corrosion inhibition efficiencies (η) associated with their strong adsorptions on metal surfaces [1,8,9].

The growing interest in Schiff bases in the field of corrosion is mainly due to their ecologically correct character and low toxicity nature, the low cost of raw materials and the use of simple synthetic routes and purification [10,11]. Further, the use of alternative methodology in the Green Chemistry field has also been attractive.

Recently, conjugated *bis*-Schiff bases, derived from 2-aminofluorene and glyoxal and 4,4'-diphenylcarboxaldehyde and 4-phthalaldehyde using traditional methodology, were evaluated in terms of inhibition effectiveness regarding corrosion of carbon steel in a HCl solution. They showed reasonable anticorrosive efficiency in the range of 58.5% to 76.8%, which was evaluated by the weight loss test at 25 °C. However, at 65 °C, the inhibition efficiency reached 98.2% after 5 h of immersion in a more active compound (*bis*-(2-aminofluorene)4,4'-biphenyldicarboxaldehyde) [12]. In addition, two double Schiff bases were evaluated regarding anticorrosive efficiency using the electrochemical impedance spectroscopy (EIS) method, gravimetric measures and topological studies of the metal surface in HCl as compared to carbon steel. Effectiveness of 88.98% and 93.00% were observed for PMB (*bis*-(2-aminofluorene)4,4'-biphenyldicarboxaldehyde) [12]. In addition, using the EIS method, two double Schiff bases, 4-(4-((pyridin-2-yl)methyleneamino)-phenoxy)-*N*-((pyridin-2-yl)methylene)-benzenamine and PPMB (4-(4-(4-((pyridin-2-yl)methyleneamino)-phenoxy)-phenoxy)-*N*-((pyridin-2-yl)methylene)-benzenamine), at 5×10^{-3} mol L⁻¹ concentration, were 88% and 92%, respectively, based on weight loss. Morphological and topological studies revealed the adsorption mode of these substances on the steel surface [13].

Also, conjugated *bis*-Schiff bases from *N*¹-(4-(4-aminophenylamino)benzene-1,4-diamine) and substituted benzaldehydes donor and withdrawals electrons [14] were investigated regarding their corrosion inhibitory effects on carbon steel in a HCl medium. Gravimetric measures, electrochemical impedance spectroscopy and a potentiodynamic polarization electrochemical test indicated the good performance of the *p*-OCH₃ substituted compound, at 250 mg L⁻¹ concentration, as these found inhibition efficiencies of 96.12%, 97.07% and 96.40%, respectively [1].

In this study, three *bis*-Schiff bases with increased saturated chains between imine-moieties (-CH=N-(CH₂)_n-N=CH-, where n = 2, 4 and 8)—namely *N,N'*-*bis*-(3-phenyl-2-propenylidene)-1,2-ethanediamine (BS2), *N,N'*-*bis*-(3-phenyl-2-propenylidene)-1,4-butanediamine (BS4) and *N,N'*-*bis*-(3-phenyl-2-propenylidene)-1,8-octanediamine (BS8)—were synthesized using an eco-friendly method, such as one that uses water as a solvent and microwave irradiation (Figure 1). These compounds were investigated as corrosion inhibitor agents for AISI 1020 carbon steel in HCl 1 mol L⁻¹. The corrosion inhibitory effectiveness of these compounds was evaluated using weight loss measures and electrochemical techniques. Further, the surface was studied using scanning electronic microscopy (SEM) and density functional theory (DFT), while the distribution of electron density in frontier molecular orbitals (FMOs) and quantum chemical data for protonated and non-protonated *bis*-Schiff bases were calculated to explore the anti-corrosion properties of these compounds. To date, these *bis*-Schiff bases have not been reported as corrosion inhibitors.

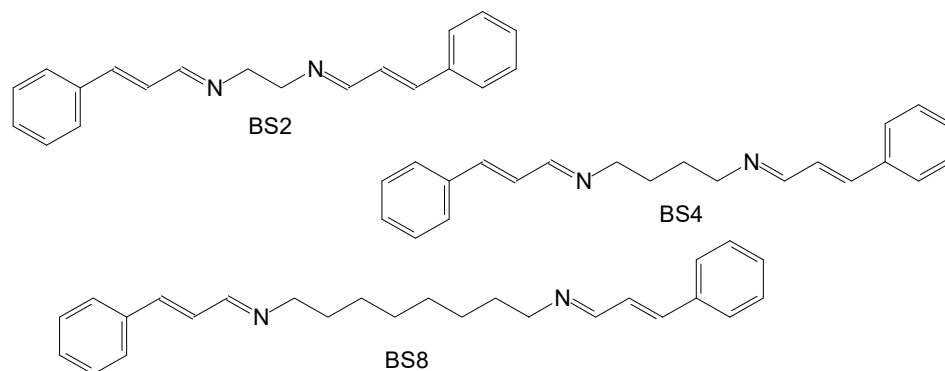


Figure 1. Molecular structures of the *bis*-Schiff bases (BS2, BS4, BS8) studied in this work.

2. Materials and Methods

2.1. Synthesis of Corrosion Inhibitors

The selected amine (ethane-1,2-, butane-1,4- and octane-1,8-diamine) was added (4 mmol) to a solution of cinnamaldehyde (8 mmol) and water. The mixture was submitted into a microwave reactor (CEM-Discover) at a potency of 80 W and 100 °C temperature for 10 min. Subsequently, the solution was cooled and the product filtrated using a vacuum, after which it was cleaned with ice water, dried and recrystallized from hexane/dichloromethane. The obtained yield was of 95–98%, and the synthetic scheme is shown in Figure 2.

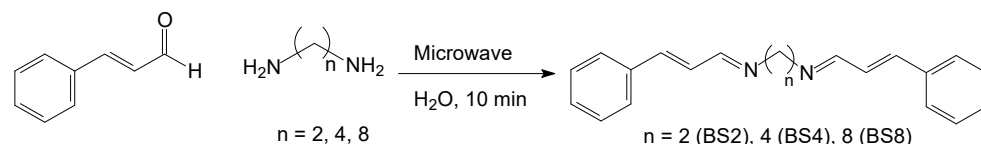


Figure 2. Synthetic scheme of the obtention of *bis*-Schiff bases BS2, BS4, BS8.

The obtained products were characterized by the FT-IR (by ATR, Bruker–Vertex 70), ^{13}C and ^1H NMR spectra on the NMR Ultrashield 500 MHz (Bruker, Billerica, MA, USA) using CDCl_3 as a solvent. The Figures 3–5 show the numbered chemical structures of BS2, BS4 and BS8, respectively. The FT-IR, ^1H and ^{13}C NMR spectra are found in the Supplementary Material.

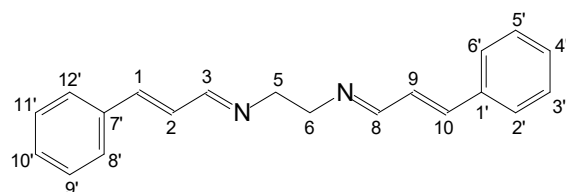


Figure 3. Characterization of the BS2 compound.

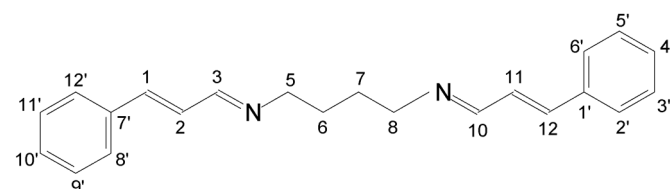


Figure 4. Characterization of the BS4 compound.

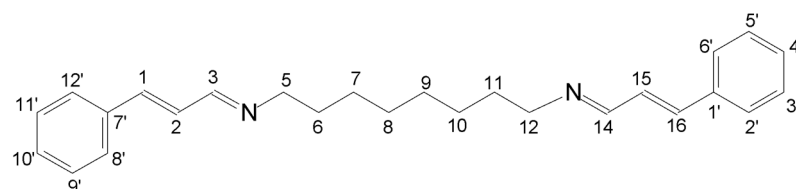


Figure 5. Characterization of the BS8 compound.

***N,N'*-Bis(3-phenyl-2-propenylidene)-1,2-ethanediamine (BS2):** 98% yield; m. p. 106 °C (lit. 101–103 °C) [15]. FT-IR (ATR, ν/cm^{-1}): 3020, 2925, 2860, 1631, 1446, 1145, 989, 748, 689, 513. ^1H NMR (500 MHz, CDCl_3) δ : 3.83 (s, 4H, H-5,6), 6.85–6.94 (m, 4H, H-1, 2, 9, 10), 7.27–7.34 (m, 6H, H-3'-5', 9'-11'), 7.44 (d, 4H, $J = 7.25$ Hz, H-2', 6', 8', 12'), 8.03 (d, 2H, $J = 7.6$ Hz, H-3, 8). ^{13}C -APT NMR (125 MHz, CDCl_3) δ : 61.7 (C-5, 6), 127.2 (C-2', 6', 8', 12'), 127.9 (C-4', 10'), 128.7 (C-2, 9), 129.0 (C-3', 5', 9', 11'), 135.6 (C-1', 7'), 141.8 (C-1, 10), 164.1 (C-3, 8).

***N,N'*-Bis(3-phenyl-2-propenylidene)-1,4-butanediamine (BS4):** 96% yield; m. p. 93 °C; FT-IR (ATR, ν/cm^{-1}) 3035, 2919, 2836, 1633, 1442, 1145, 981, 750, 688, 513; ^1H NMR (500 MHz, CDCl_3) δ : 1.73 (s, 4H, H-6, 7), 3.56 (s, 4H, H-5,8), 6.85–6.96 (m, 4H, H-1, 2, 11, 12), 7.29–7.37 (m, 6H, H-3'-5', 9'-11'), 7.47 (d, 4H, $J = 8.8$ Hz, H-2', 6', 8', 12'), 8.03 (d, 2H, $J = 9.1$ Hz, H-3, 10); ^{13}C -APT NMR (125 MHz, CDCl_3) δ : 28.9 (C-6, 7), 61.6 (C-5, 8), 127.4 (C-2', 6', 8', 12'), 128.4 (C-4',10') 129.1 (C-2, 11), 129.3 (C-3', 5', 9', 11'), 136.0 (C-1', 7'), 141.7 (C-1, 12), 163.0 (C-3, 10).

***N,N'*-Bis(3-phenyl-2-propenylidene)-1,8-octanediamine (BS8):** 95% yield; m. p. 65 °C. FT-IR (ATR, ν/cm^{-1}): 3021, 2928, 2845, 1631, 1441, 1150, 970, 748, 691, 519. ^1H NMR (500 MHz, CDCl_3) δ : 1.33 (s, 8H, H-7–10), 1.64 (s, 4H, H-6, 11), 3.49 (t, 4H, H-5, 12), 6.85–6.93 (m, 4H, H-1, 2, 15, 16), 7.28–7.36 (m, 6H, H-3'-5', 9'-11'), 7.46 (d, 2H, $J = 7.5$ Hz, H-2', 6', 8', 12'), 8.0 (d, 2H, $J = 6.6$ Hz, H-3, 14); ^{13}C -APT NMR (125 MHz, CDCl_3) δ : 27.3 (C-8, 9), 29.3 (C-7, 10), 30.8 (C-6, 11), 61.6 (C5, 12), 127.1 (C-2', 6', 8', 12'), 128.3 (C-4', 10'), 128.7 (C-2, 15), 130.0 (C-3', 5', 9', 11'), 135.8 (C-1', 7'), 141.1 (C-1, 16), 162.3 (C-3, 14).

2.2. Electrochemical Measurements

The electrochemical measures took place in a HCl solution (1 mol L^{-1}) with the lack (Blank) and presence of *bis*-Schiff bases in four concentrations (1.0×10^{-3} to $1.0 \times 10^{-6} \text{ mol L}^{-1}$). All tests were conducted at 30 °C and employed an electrochemical cell containing three electrodes: AISI 1020 carbon steel embedded in resin, with an exposed area of 1.0 cm^2 , constituted the working electrode with an auxiliary electrode of platinum and a silver chloride electrode ($\text{Ag(s)}/\text{AgCl(s)}/\text{Cl}^-$ (3.0 mol L^{-1})) as references.

The electrode surface, before immersion in the aggressive solution, was processed by abrasion with sandpaper till it was up to 2000 grade. Finally, the excess fat was removed using ethanol, and it was cleaned using purified water and dried. All electrochemical corrosion assays were executed in an open system employing the Autolab Potentiostat/Galvanostat (model PGSTAT 302N), and the program used was NOVA 2.1.

2.2.1. Electrochemical Impedance Spectroscopy (EIS)

After 60 min of open circuit potential (E_{ocp}), impedance data were obtained at a 10 kHz to 0.1 Hz frequency interval with an amplitude of 10 mV between the peaks. The efficiency (η_{EIS}) of the inhibitor was calculated using Equation (1).

$$\eta_{\text{EIS}}(\%) = \frac{R_{\text{ct}} - R_{\text{ct}}^0}{R_{\text{ct}}} \times 100 \quad (1)$$

where R_{ct} and R_{ct}^0 are the charge transfer resistances in the presence and in the absence of the compound, respectively.

2.2.2. Linear Polarization Resistance (LPR)

LPR measurements were carried out by employing 1 mV s^{-1} as the scan rate in the interval of potential at an E_{ocp} of around $\pm 10 \text{ mV}$. The inhibition efficiency (η_{LPR}) was calculated using Equation (2).

$$\eta_{\text{LPR}}(\%) = \frac{R_{\text{p}} - R_{\text{p}}^0}{R_{\text{p}}} \times 100 \quad (2)$$

where R_{p} and R_{p}^0 are the resistance of polarization with the addition of the synthesized compounds and in the Blank, respectively, and η_{LPR} is the percentage of efficiency. The values of R_{p} correspond to the angular coefficients calculated using the linear regression of the plot of current density (i) versus potential (E).

2.2.3. Potentiodynamic Polarization (PP)

PP measurements were executed by applying 1 mV s^{-1} of scan rate in the $\pm 200 \text{ mV}$ potential range on all sides of the open circuit potential (E_{ocp}). The efficiency (η_{PP}) of the inhibitor was calculated using Equation (3).

$$\eta_{\text{PP}} (\%) = \frac{i_{\text{corr}}^0 - i_{\text{corr}}}{i_{\text{corr}}^0} \times 100 \quad (3)$$

where i_{corr}^0 is the value of the density of the solution without the synthesized compounds, i_{corr} is the inhibited corrosion density and η_{PP} is the percentage of corrosion inhibition efficiency.

2.3. Weight Loss Method

The weight loss method measures were performed using samples of carbon steel, AISI 1020, sized $3.0 \times 3.0 \times 0.15 \text{ cm}$ in a 1 mol L^{-1} of HCl solution in the lack and presence of the *bis*-Schiff bases in concentrations of 1.0×10^{-5} to $1.0 \times 10^{-3} \text{ mol L}^{-1}$ with immersion times of 3, 24 and 48 h and naturally aerated at $30 \text{ }^\circ\text{C}$. The temperature effect was studied using 3 h of immersion at 30, 40, 50 and $60 \text{ }^\circ\text{C}$.

Before each assay, the samples were worn down using 100, 400 and 600 grade sandpaper, degreased with ethanol, cleaned with distilled water, and dried. After immersion tests, pickling and weighing were performed. The efficiency (η_{WL}) of the inhibition was calculated using Equation (4).

$$\eta_{\text{WL}} (\%) = \frac{W_0 - W}{W_0} \times 100 \quad (4)$$

where W_0 is the rate in the solution without the compound, and W is the corrosion rate in the presence of the studied inhibitors.

2.4. Surface Investigation

Scanning Electron Microscopy

Carbon steel coupons ($3.0 \times 3.0 \times 0.15 \text{ cm}$) were polished using 100-, 400- and 600-degree sandpaper, degreased with ethyl alcohol, washed with purified water, dry, and submerged in a HCl solution (1 mol L^{-1}) with BS2, BS4 and BS8 and without (Blank) for 24 h at $30 \text{ }^\circ\text{C}$. The coupons were detached, cleaned with water and dried using hot air. The results were acquired using a HITACHI TM 3000 Tabletop Microscope.

2.5. Theoretical Calculations

To improve our comprehension of the corrosion inhibition of the di-protonated molecules, we conducted density functional theory (DFT) calculations employing the B3LYP functional and the def2-QZVP basis group within Orca software [16–18]. The conductor-like polarizable continuum model (CPCM) [19] was employed to simulate the molecular environment in a solution, as solvents can impact reactive properties. A dielectric constant of $\epsilon = 60.75$ characterized the implicit solvent. We explored the relation between corrosion inhibition effectiveness and electronic and structural properties through reactivity molecular descriptors, including the energy value of the highest occupied molecular orbital (E_{HOMO}), the energy value of the LUMO (E_{LUMO}), the HOMO-LUMO energy gap (ΔE_{gap}), the ionization potential (I), the electronegativity (χ), the electron affinity (A), the global softness (σ), the global hardness (η), the fraction of electrons transferred (ΔN), the global electrophilicity index (ω) and the nucleophilicity index (ϵ). The molecular sketches of the input were drawn using Avogadro version 1.2 [20], and the results were analyzed using the trial version of ChemCraft version 1.8 [21].

In agreement with Koopman's theorem [22], the ionization potential (I) can be defined as a function of E_{HOMO} (Equation (5)), whereas electron affinity (A) is defined in terms of E_{LUMO} (Equation (6)).

$$I = -E_{\text{HOMO}} \quad (5)$$

$$A = -E_{\text{LUMO}} \quad (6)$$

Electronegativity (χ) is described as a derivative of the total electronic energy of the system (E) with respect to the total number of electrons (N) at constant external potential (v) (Equation (7)). Therefore, it can be simply described as a function of the ionization potential (I) and electron affinity (A) [23], according to Equation (8).

$$\chi = -\left(\frac{\partial E}{\partial N}\right)_v \quad (7)$$

$$\chi = \left(\frac{I + A}{2}\right) \quad (8)$$

The absolute hardness or global hardness (η) of an N -electrons system at external potential v is defined in Equation (9). It can be expressed as a function of the ionization potential and electron affinity according to Equation (10) [24,25]. The global softness (σ) is the reciprocal of absolute hardness, as given by Equation (11).

$$\eta = \left(\frac{\partial^2 E}{\partial N^2}\right)_v \quad (9)$$

$$\eta = \left(\frac{I - A}{2}\right) \quad (10)$$

$$\sigma = \left(\frac{1}{\eta}\right) \quad (11)$$

The global electrophilicity index (ω) and nucleophilicity index (ε) were evaluated according to Equations (12) and (13), respectively [26].

$$\omega = \left[\frac{(I + A)^2}{8(I - A)}\right] \quad (12)$$

$$\varepsilon = \left(\frac{1}{\omega}\right) \quad (13)$$

The portion of electrons transferred (ΔN) from the compound to the metallic surface is defined by Equation (14) [27].

$$\Delta N = \left[\frac{\chi_M - \chi_{\text{inh}}}{2(\eta_M + \eta_{\text{inh}})}\right] \quad (14)$$

In the given context χ represents the electronegativity, η denotes the global hardness, and M refers to the metallic surface, while the subscript "inh" indicates the inhibitor molecule.

In order to study the specific interactions among the inhibitor and the metal, we conducted periodic spin-polarized density functional theory (DFT) calculations using the Quantum ESPRESSO [28] plane wave package. The Perdew–Burke–Ernzerhof (PBE) exchange–correlation functional was employed [29]. The ultrasoft pseudopotentials developed by Vanderbilt [30] were utilized, and a limit energy of 70 Ry was applied to the plane wave basis group. To guarantee precise results, the Brillouin zone was sampled with a Monkhorst-Pack [31] k -point mesh of $8 \times 8 \times 8$ for the bulk material. This sampling method yielded good agreement with experimental data as evidenced by the equilibrium

lattice constant (2.88 Å) and the magnetic moment (2.32 μB), which closely matched the experimental values of 2.86 Å and 2.22 μB , respectively [32].

For the Fe(110) surface, which is considered the most stable iron surface [33], a Monkhorst-Pack grid of $2 \times 2 \times 1$ was employed. To accommodate the BS2, BS4 and BS8 inhibitors with the Fe(110) surface, a supercell expansion of 7×7 was found to be adequate. The slab consisted of three iron layers, with the top layer allowed to relax while the bottom two layers remained fixed. To prevent interactions with non-periodic axis periodic images, a vacuum thickness of 20 Å was implemented. In all calculations, the D3 long-range correction was utilized as it is known to be crucial in studying the adsorption of aromatics on metal surfaces [34–36]. To balance the charge of the double protonated surface-inhibitor systems, two counteranions (2Cl^-) were employed. For calculations involving isolated molecules, a cubic cell of 30 Å was used, and the Makov–Payne correction was applied [37].

3. Results

3.1. Synthesis

The green synthesis of B2, B4 and B8 was performed in one step by mixing cinnamaldehyde with the selected amine in water as a solvent. The reaction mixture was refluxed for 10 min in a microwave reactor with 80 W of potency. At the end of the reaction, a brown oil was obtained, which turned into a yellow solid. After cooling, it was isolated and treated with cold water, dried and purified by recrystallization with a hexane/dichloromethane mixture. The products were obtained with 95–98% of yield. The *bis*-Schiff bases were characterized by routine spectroscopies such as FT-IR and NMR (^1H and ^{13}C).

In the infrared spectra (FT-IR) of BS2, BS4 and BS8 aromatic C-H stretching characteristic bands were observed in the range of 3020–3035 cm^{-1} and aliphatic characteristic bands in the range of 2919–2860 cm^{-1} . The absorption of the C=N stretching of imine moiety was in the range of 1631–1633 cm^{-1} , and a band referring to the angular deformation of five adjacent hydrogens of the aromatic ring was observed at 748–750 cm^{-1} .

The ^1H NMR spectra for BS2 were seen at δ 3.83 (4H, H-5, 6), referring to the chemical shifts of hydrogens in the aliphatic chain. In the range of δ 6.85–6.94 (4H, H-1, 2, 9, 10), signals from olefinic hydrogens were observed, and δ 7.27–7.34 (6H, H-3'-5', 9'-11'), δ 7.44 (4H, $J = 7.25$, H-2', 6', 8', 12') were assigned the chemical shifts of aromatic hydrogens. At δ 8.03, a signal referring to the chemical shift of imine hydrogen was observed. In the ^{13}C NMR spectrum, a signal was observed at δ 61.7 (C-5, 6), referring to the aliphatic carbons and at δ 128.7 (C-2, 9) and 141.8 (C-1, 10), signals referring to olefinic carbons. The displacements attributed to aromatic hydrogens were observed in the range of δ 127.2–135.6 and the signal referring to the imine carbon at δ 164.1 (C-3, 8).

The BS4 compound showed signals at δ 1.73 (4H, H-6, 7) and δ 3.56 (4H, H-5, 8), referring to the chemical shifts of hydrogens in the aliphatic chain, and in the range of δ 6.85–6.94 (4H, H-1, 2, 11, 12) to the olefin hydrogens. δ 7.29–7.37 (6H, H-3'-5', 9'-11') and δ 7.47 (4H, $J = 8.8$, H-2', 6', 8', 12') were attributed to the chemical shifts of aromatic hydrogens, and the signal referring to the chemical shift of the imine hydrogen was observed at δ 8.03. In the ^{13}C NMR spectrum, signals were observed at δ 28.9 (C-6, 7) and 61.7 (C-5, 8), referring to aliphatic carbons, and δ 129.1 (C-2, 11) and δ 141.7 (C-1, 12) to olefinic carbons. The displacements related to aromatic carbons were attributed at δ 127.4 (C-2', 6', 8', 12'), δ 128.4 (C-4', 10'), δ 129.3 (C-3', 5', 9', 11'), and δ 135.6 (C-1', 7'). The signal referring to the imine carbon was observed at δ 163.0 (C-3, 10).

For the BS8 compound, signals at δ 1.33 (8H, 7–10), δ 1.64 (4H, H-6, 11) and δ 3.49 (4H, H-5, 12) were attributed to the hydrogens in the aliphatic chain and in the range of δ 6.85–6.93 (4H, H-1, 2, 15, 16) to olefinic hydrogens. The chemical shifts at δ 7.28–7.36 (6H, H-3'-5', 9'-11') and δ 7.46 (4H, $J = 7.5$, H-2', 6', 8', 12') were assigned to the aromatic hydrogens and at δ 8.0 to the imine hydrogen. In the ^{13}C NMR spectrum, signals were observed at δ 27.3 (C-8, 9), δ 29.3 (C-7, 10), 30.8 (C-6, 11) and δ 61.6 (C-5, 12), referring to aliphatic carbons and at δ 128.7 (C-2, 15) and δ 141.1 (C-1, 16) to olefinic carbons. The

displacements related to aromatic carbons were observed at δ 127.1 (C-2', 6', 8', 12'), δ 128.2 (C-4', 10'), δ 130.0 (C-3', 5', 9', 11') and δ 135.8 (C-1', 7') and the signal referring to the imine carbon at δ 162.3 (C-3, 14).

The FT-IR, ^1H and ^{13}C NMR spectra can be seen in the Supplementary Material.

3.2. EIS

This method is used to study the corrosion process, inhibitor efficiency and charge transfer mechanism that occur between the metal–solution interface. In this work, Nyquist and Bode plots were obtained from the EIS of carbon steel submerged in HCl (1 mol L^{-1}) with and without *bis*-Schiff bases at the concentration levels of 1.0×10^{-3} , 1.0×10^{-4} , 1.0×10^{-5} and $1.0 \times 10^{-6} \text{ mol L}^{-1}$ at $30 \text{ }^\circ\text{C}$. Before each EIS measurement, the E_{ocp} was monitored for 60 min since this immersion time is enough to achieve the stability condition of the E_{ocp} , as demonstrated by the plots in Figure 6.

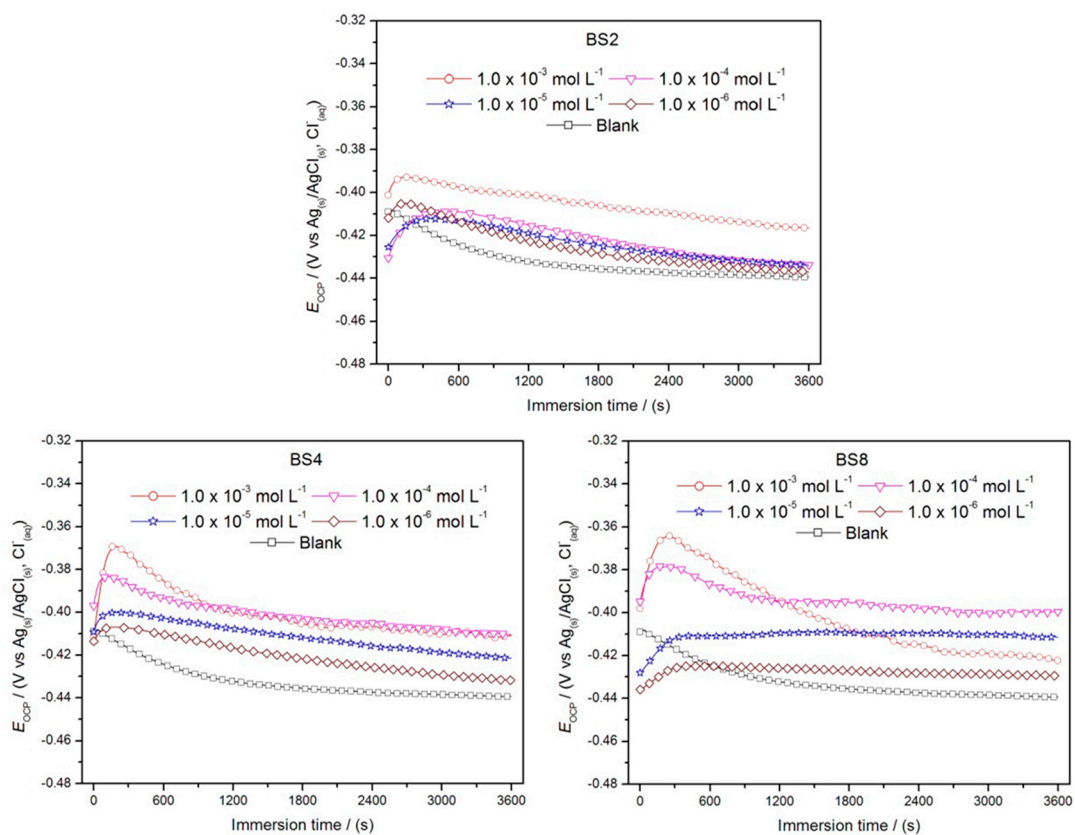


Figure 6. The shift of E_{oc} values with the immersion time obtained for the AISI 1020 carbon steel in HCl (1 mol L^{-1}) in the Blank and with the addition of the studied inhibitor agents: BS2, BS4, and BS8.

Afterward, the impedance data were obtained, and they are displayed in the Nyquist (Figure 7) and Bode (Figure 8) plots. For the Nyquist plots (Figure 7), it can be noted that the semicircle diameters obtained in the presence of the BS2, BS4 and BS8 inhibitors were higher than that achieved in the Blank. The increase in the semicircle diameter was also observed with a greater number of molecules, which is attributed to a rise in the surface coverage (θ). Moreover, the profiles of the Nyquist plots were unchanged with inhibitor addition since all the Nyquist plots presented only capacitive arcs and there was no unique time change in the Bode graph, showing that the process is commanded by a charge-carrying event and that the hydrogen evolution is the predominant cathodic reaction [38,39].

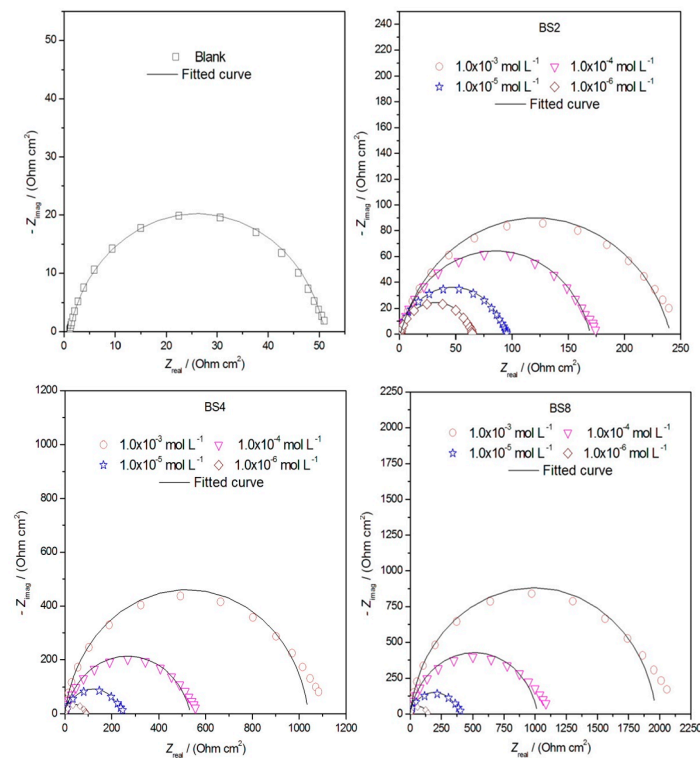


Figure 7. Nyquist plots acquired for the BS2, BS4 and BS8 inhibitors in an acid medium at 30 °C.

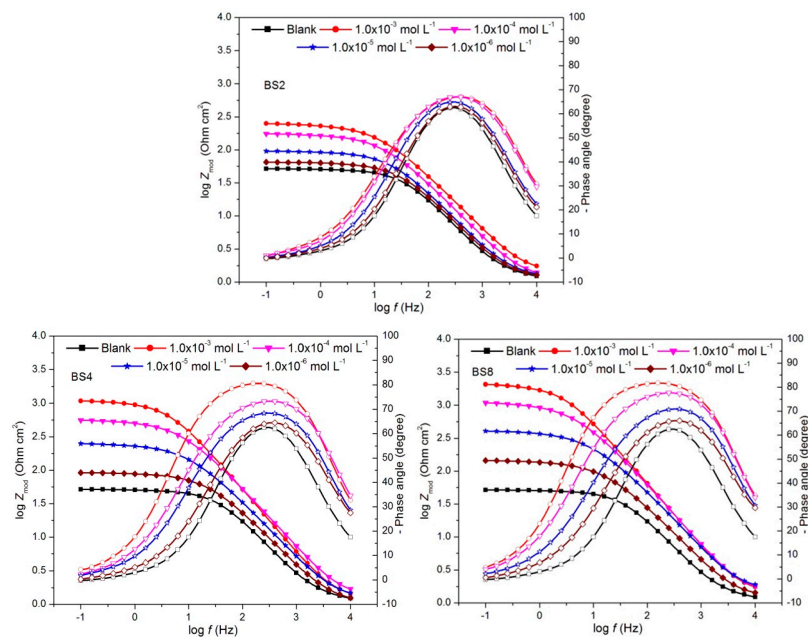


Figure 8. Bode plots obtained for AISI 1020 carbon steel immersed in HCl (1 mol L⁻¹) and with the lack of and with BS2, BS4 and BS8 presence at 30 °C.

The θ value is relative to the corrosion inhibition efficiency and is obtained by Equation (15):

$$\theta = \frac{R_{ct} - R_{ct}^0}{R_{ct}} \quad (15)$$

where R_{ct} is the charge transfer resistance in the Blank and R_{ct}^0 in that with the addition of the *bis*-Schiff bases acquired by EIS [38,39].

The depressive semicircle observed on the Z_{real} axis at the lowest frequency can be related to the small rugosity and lack of homogeneity of the metal surface [40]. Thereby, the CPE was applied for more fitting accuracy, which has R_{ct} and the constant phase element of the double layer in parallel with the two in series with solution resistance [41]. All impedance data were adjusted using the equivalent electric circuit shown in Figure 9.

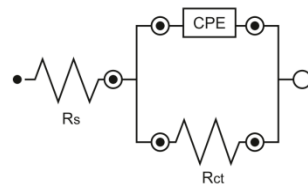


Figure 9. Equivalent electric circuit used to adjust for impedance data.

The CPE, constant phase element, is represented in Equation (16):

$$Z_{\text{CPE}} = Y_0^{-1} (j\omega)^{-n} \quad (16)$$

where: Y_0 = size of the CPE, j = imaginary unit, ω = angular frequency and n = phase shifting.

The double layer capacitance (C_{dl}) derived from the CPE values can be calculated by Equation (17):

$$C_{\text{dl}} = Y_0 (2\pi f_{\text{max}})^{n-1} \quad (17)$$

where: f_{max} = frequency related to the imaginary part of the highest impedance [42,43].

The electrochemical data acquired using EIS are shown in Table 1, and the increase of R_{ct} values with the augment of concentration for all investigated compounds can be noted. This is due to the adsorption of the compounds into the metal surface, resulting in fewer sites being available for corrosion [40,41]. The BS8 compound in the highest concentration showed a higher value on the Z_{real} axis of the Nyquist diagram with 98% of corrosion inhibition efficiency. Under similar conditions, the *bis*-Schiff base, with a more complex structure—4-(4-(4-((pyridin-2-yl)-methyleneamino)-phenoxy)-phenoxy)-*N*-((pyridin-2-yl)-methylene)-benzenamine—showed 93% of inhibition efficiency at $5.0 \times 10^{-3} \text{ mol L}^{-1}$ of concentration [13].

Table 1. Impedance parameters for AISI 1020 carbon steel in a HCl solution (1 mol L^{-1}) in the lack and presence of BS2, BS4 and BS8. The impedance data were obtained at $30 \text{ }^\circ\text{C}$.

Compound	C_{inh} (mol L^{-1})	OCP/ Ag/AgCl (mV)	R_{ct} ($\Omega \text{ cm}^2$)	n	Y_0 ($\mu\text{Ohm cm}^{-2}$)	f_{max} (Hz)	C_{dl} ($\mu\text{F cm}^{-2}$)	Θ	$\eta_{\text{EIS}} \pm \text{SD}$ (%)
Blank	-	-436	50	0.869	200	31.6	99	-	-
	1.0×10^{-6}	-437	63	0.847	205	31.6	91	0.206	21.1 ± 0.7
BS2	1.0×10^{-5}	-434	92	0.843	190	19.95	89	0.456	46.0 ± 0.3
	1.0×10^{-4}	-434	169	0.829	152	12.58	72	0.704	70.2 ± 0.6
	1.0×10^{-3}	-417	239	0.819	127	10.0	60	0.790	79.1 ± 0.3
	1.0×10^{-6}	-432	90	0.828	197	19.95	86	0.444	44.3 ± 0.4
BS4	1.0×10^{-5}	-422	245	0.831	142	10.00	70	0.796	79.2 ± 0.9
	1.0×10^{-4}	-411	549	0.858	77	6.30	45	0.908	91.6 ± 0.5
	1.0×10^{-3}	-411	1043	0.924	51	3.98	40	0.952	95.4 ± 0.8
	1.0×10^{-6}	-422	138	0.823	174	15.84	77	0.637	64.1 ± 0.7
BS8	1.0×10^{-5}	-411	410	0.841	95	7.94	51	0.878	88.1 ± 0.8
	1.0×10^{-4}	-411	1058	0.889	55	3.98	38	0.952	95.4 ± 0.3
	1.0×10^{-3}	-422	2069	0.930	39	2.51	31	0.976	98.3 ± 0.4

SD: standard deviation.

As shown in Table 1, a decrease of C_{dl} values is observed as the concentration increases, reflecting the decrease of the site dielectric constant, which is assigned to the interaction of the inhibitors on the metal surface by displacing previously adsorbed molecules of water [44] and also by the increasing the thickness of the double layer.

3.3. LPR

The LPR measurements were executed in similar conditions as those of the EIS tests, and the results regarding the corrosion inhibition efficiencies were acquired in the same range. The values acquired from the LPR tests were calculated after using linear regression in the graph of corrosion potential (E) versus current density (i). The polarization resistance (R_p) data and inhibition efficiencies (η_{LPR}) are displayed in the Table 2.

Table 2. The LPR data for AISI 1020 carbon steel in a solution of HCl (1.0 mol L^{-1}) in the lack and presence of BS2, BS4 and BS8. The LPR measurements were carried out at $30 \text{ }^\circ\text{C}$.

Compound	C_{inh} (mol L^{-1})	$E_{oc}/$ (mV)	R_p ($\Omega \text{ cm}^2$)	Θ	$\eta_{LPR} \pm \text{SD}$ (%)
Blank	-	-441	52	-	-
	1.0×10^{-6}	-439	63	0.174	17.2 ± 0.5
BS2	1.0×10^{-5}	-436	97	0.464	46.1 ± 0.3
	1.0×10^{-4}	-436	176	0.704	70.4 ± 0.6
	1.0×10^{-3}	-420	244	0.786	79.0 ± 0.6
	1.0×10^{-6}	-435	93	0.440	44.2 ± 0.7
BS4	1.0×10^{-5}	-425	325	0.840	84.1 ± 0.3
	1.0×10^{-4}	-413	557	0.906	91.6 ± 0.3
	1.0×10^{-3}	-413	1155	0.955	95.1 ± 0.7
	1.0×10^{-6}	-424	149	0.651	64.3 ± 0.7
BS8	1.0×10^{-5}	-413	416	0.875	88.2 ± 0.9
	1.0×10^{-4}	-401	1118	0.953	95.4 ± 0.1
	1.0×10^{-3}	-414	1915	0.972	97.6 ± 0.4

SD: standard deviation.

The R_p values were enhanced with that of the concentration, suggesting that the compounds adsorbed on active locations of the metallic surface formed a covering layer according to the R_{ct} values acquired using the EIS method.

As shown in Table 2, the BS8 compound also showed the best corrosion inhibition efficiency, 97%, at $1.0 \times 10^{-3} \text{ mol L}^{-1}$ concentration, according to the results acquired by the EIS assays. Figure 10 shows the comparison of BS2, BS4 and BS8 in terms of the inhibition efficiency \times concentration.

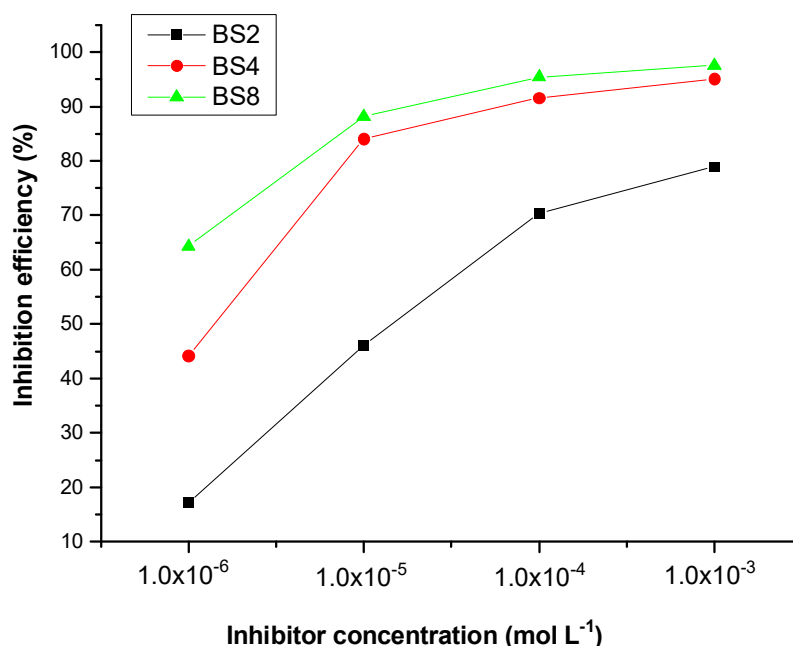


Figure 10. Comparison of BS2, BS4 and BS8 in terms of the inhibition efficiency \times concentration.

3.4. PP

The PP experiments were conducted at 30 °C in the same acid solution conditions in the lack and presence of BS2, BS4 and BS8. The curves obtained for the metallic surface in the acidic solution in the lack and presence of the corrosion inhibitors are displayed in Figure 11. According to Equation (3), the efficiency was calculated based on the current density in the presence of the inhibitor (i_{corr}) and the current density in the absence of the inhibitor (i_{corr}^0), providing the efficiency value in percentage η_{PP} .

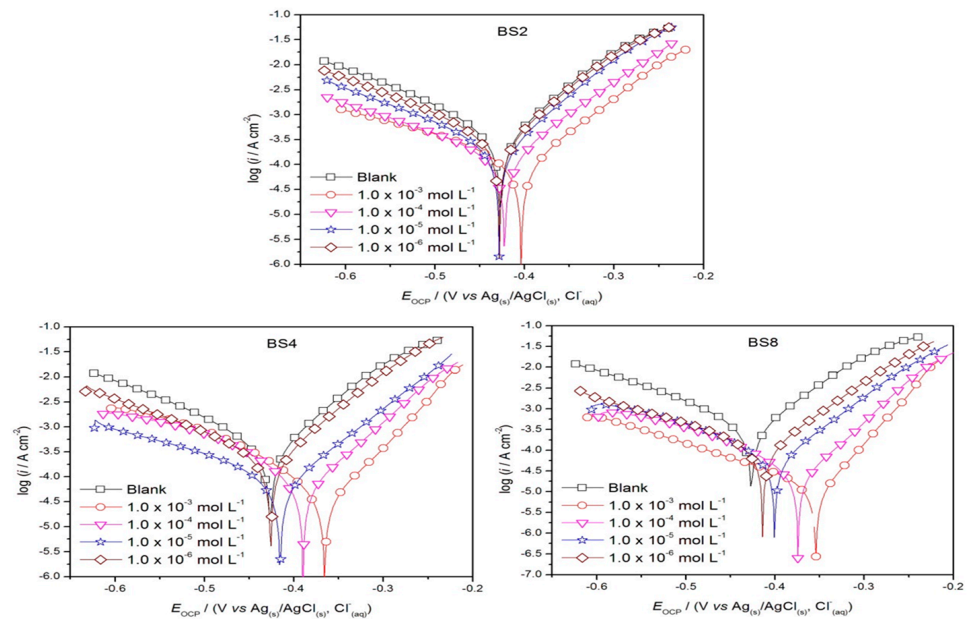


Figure 11. Tafel curves of AISI 1020 carbon steel in a hydrochloric acid solution (1.0 mol L^{-1}) in the lack and presence of BS2, BS4 and BS8.

The polarization curves show that the presence of the corrosion inhibitors leads to a reduction of current densities in both cathodic and anodic reactions in comparison with those displayed in the Blank. Furthermore, both cathodic and anodic Tafel lines are parallel, showing that the inclusion of the compounds does not modify the mechanism of corrosion in both cathodic and anodic reactions. Finally, for an elevated amount of the inhibitors, a greater movement of E_{corr} in the anodic branch was also noted.

The obtained results suggest that these substances act as a miscellaneous form of corrosion inhibitors with anodic tendencies that can delay metal dissolution in cathodic reactions [43]. The presence of the compounds in the acid solution decreased the steel oxidation rate and delayed the evolution of hydrogen in the anodic direction as well, retarding the dissolution of the metal. However, a slight shift in the anodic direction can be observed, showing a greater tendency to protect the metal. The best results were observed for BS8, mainly at $1.0 \times 10^{-3} \text{ mol L}^{-1}$ concentration. Table 3 shows the data derived from the polarization curves.

It is well known that the π bond, aromatic rings and imine group are very important in the adsorption of organic compounds into the carbon steel surface [1,45]. In this work, the studied compounds differ only by length of alkyl chains, which have two, four or eight saturated carbons. Thus, the lengthening of the alkyl chain may be responsible for the increments in corrosion inhibition efficiency due to the increase of the liberty degrees in the alkyl portion that favors the interaction of the two C=N groups in the metallic surface.

Table 3. PP parameters for AISI 1020 carbon steel in a hydrochloric acid solution (1.0 mol L⁻¹) in the absence and presence of BS2, BS4 and BS8.

Compound	C _{inh} (mol L ⁻¹)	E _{corr} vs. Ag/AgCl (mV)	j _{corr} (mA cm ⁻²)	β _a (mV dec ⁻¹)	-β _c (mV dec ⁻¹)	Θ	η _{PP} ± SD (%)
Blank	-	-427	0.314	71	101	-	-
	1.0 × 10 ⁻⁶	-427	0.255	69	110	0.188	19.4 ± 0.8
BS2	1.0 × 10 ⁻⁵	-427	0.188	70	117	0.401	40.1 ± 0.5
	1.0 × 10 ⁻⁴	-422	0.145	82	161	0.538	54.0 ± 0.5
	1.0 × 10 ⁻³	-402	0.102	85	133	0.675	67.1 ± 0.2
	1.0 × 10 ⁻⁶	-425	0.203	71	118	0.354	35.3 ± 0.2
BS4	1.0 × 10 ⁻⁵	-415	0.066	76	117	0.789	79.6 ± 0.6
	1.0 × 10 ⁻⁴	-389	0.054	67	75	0.828	83.2 ± 0.5
	1.0 × 10 ⁻³	-365	0.032	61	69	0.898	90.1 ± 0.5
	1.0 × 10 ⁻⁶	-413	0.113	74	134	0.640	64.4 ± 0.5
BS8	1.0 × 10 ⁻⁵	-400	0.052	64	90	0.834	83.2 ± 0.9
	1.0 × 10 ⁻⁴	-374	0.017	52	67	0.946	95.0 ± 0.1
	1.0 × 10 ⁻³	-354	0.008	43	80	0.974	97.4 ± 0.8

E_{corr}: energy of corrosion; j_{corr}: corrosion current density; β_a and β_c: anodic and cathodic Tafel constants, respectively; Θ: degree of coverage surface; SD: standard deviation.

The parameters associated with polarization curves, such as energy of corrosion (E_{corr}), corrosion current density (j_{corr}), inhibitor coverage degree (Θ) and anodic and cathodic Tafel constants (β_a and β_c, respectively), were obtained by the extrapolation of the linear portions of the curves of the anodic and cathodic polarization lines [46]. The efficiency of inhibition η_{PP} (%) and the other parameters obtained by PP are shown in Table 3.

3.5. Adsorption Phenomenon

The isotherms can provide important details about the features of interactions between the metallic surface and corrosive medium containing the inhibitor [47]. As previously observed, inhibition efficiencies increase with increasing concentration values, also leading to the enlargement of the degree of surface coverage (θ) by inhibitor presence. Thus, the θ values, obtained from EIS, were fitted against concentration according to some models of adsorption isotherms like Langmuir [48,49], Temkin [50], Frumkin [51] and El-Awady [50] (Equations (18)–(21)). Table 4 shows the obtained regression parameters of the correlation coefficient (r) and slope for the Langmuir, Temkin, Frumkin and El-Awady adsorption isotherms for BS2, BS4 and BS8 added to carbon steel in a HCl solution.

$$\text{Langmuir isotherm equation : } \frac{C}{\theta} = \frac{1}{K_{\text{ads}}} + C \quad (18)$$

$$\text{Temkin isotherm equation : } \theta = -\frac{\ln K_{\text{ads}}}{2a} - \frac{\ln C}{2a} \quad (19)$$

$$\text{umkin isotherm equation : } \ln \frac{\theta}{(1-\theta)} = \ln K_{\text{ads}} + 2a \quad (20)$$

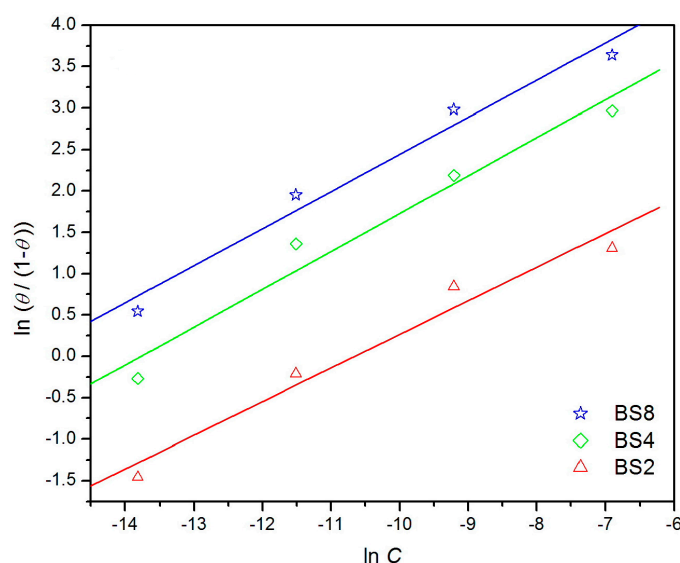
$$\text{El - Awady isotherm equation : } \ln \frac{\theta}{(1-\theta)} = \ln K' + y \ln C \quad (21)$$

where θ is the degree of coverage surface, C is the concentration, K' is the apparent equilibrium adsorption constant, y is the number of molecules present in an active location, and K_{ads} the equilibrium adsorption constant.

Table 4. Parameters obtained from the Langmuir, Temkin, Frumkin and El-Awady adsorption isotherms for BS2, BS4 and BS8 added to AISI 1020 carbon steel in a HCl solution.

Adsorption Isotherm	Inhibitor	Correlation Coefficient	Slope (y)	$1/y$
Langmuir	BS2	0.999	1.02	-
	BS4	0.999	1.04	-
	BS8	0.999	1.26	-
Temkin	BS2	0.980	0.08	-
	BS4	0.880	0.07	-
	BS8	0.908	0.04	-
Frumkin	BS2	0.946	-6.25	-
	BS4	0.746	-5.36	-
	BS8	0.847	-8.96	-
El-Awady	BS2	0.982	0.41	2.43
	BS4	0.982	0.45	2.22
	BS8	0.987	0.45	2.22

Table 4 shows good correlation coefficient (r) for the Langmuir and El-Awady adsorption isotherms. However, the slopes obtained from the Langmuir isotherm, especially for BS8, were different from that of the unit, suggesting that the adsorption does not occur homogeneously—i.e., a monolayer film is not formed, and possible interactions occur between the molecules. However, the El-Awady adsorption isotherm is an adjusted model of the Langmuir equation that indicates the capacity of compounds that interact with more sites on the metal surface [52,53]. Figure 12 shows the graph with the El-Awady adsorption isotherms.

**Figure 12.** The El-Awady adsorption isotherms plot for BS2, BS4 and BS8 added to the AISI 1020 surface in a 1.0 mol L⁻¹ HCl solution.

In accordance with Table 4, the interaction parameters $1/y$ (number of active local sites of the metal occupied by an inhibitor) showed values around 2, which means that each molecule occupies nearly two active metal sites. Thus, it is concluded that each imine portion conjugated to the aromatic ring occupies two active sites of the metal.

From the K' parameter obtained by the El-Awady adsorption isotherm equation, it was possible to evaluate the adsorption equilibrium constant (K_{ads}) values in relation to the organic compounds using the ratio $K_{\text{ads}} = K'^{1/y}$ and the adsorption free energy (ΔG_{ads}^0) using Equation (22):

$$\Delta G_{\text{ads}}^0 = -RT \ln(55.55 K_{\text{ads}}) \quad (22)$$

where T is the temperature (K), R is the universal gas constant ($\text{J K}^{-1} \text{mol}^{-1}$), and 55.55 is the value of molar concentration of water in the acidic medium. Table 5 shows the K_{ads} and ΔG_{ads}^0 obtained for BS2, BS4 and BS8.

Table 5. Values of K_{ads} and ΔG_{ads}^0 obtained for BS2, BS4 and BS8 added to carbon steel in a HCl solution (1.0 mol L^{-1}).

Inhibitor	K_{ads}	ΔG_{ads}^0 (kJ mol^{-1})
BS2	3.70×10^4	−36.02
BS4	12.01×10^5	−44.63
BS8	47.17×10^5	−48.03

The great values of K_{ads} indicate an elevated adsorption of compounds on the metallic surface, and the ΔG_{ads}^0 with negative values displays a highly spontaneous process of corrosion limitation of these substances. The BS8 compound has the highest K_{ads} and most negative ΔG_{ads}^0 values due to better interactions between the inhibitor compound and metallic surface, justifying it having the best anticorrosion efficiency.

3.6. Weight Loss Method

3.6.1. Immersion Time Effect

The weight loss measures were performed using AISI 1020 carbon steel in hydrochloric acid (1.0 mol L^{-1}) in the lack and presence of BS2, BS4 and BS8 in three concentrations (1.0×10^{-3} , 1.0×10^{-4} , $1.0 \times 10^{-5} \text{ mol L}^{-1}$), with immersion times of 3, 24 and 48 h and naturally aerated at $30 \text{ }^\circ\text{C}$. The results obtained are displayed in Table 6.

Table 6. Weight loss results obtained for AISI 1020 carbon steel in a HCl solution in the lack and presence of BS2, BS4 and BS8 at $30 \text{ }^\circ\text{C}$ with three immersion times.

Inhibitor (mol L^{-1})	3 h		24 h		48 h		
	W_{corr} ($\text{mg cm}^{-2} \text{ h}^{-1}$)	$\eta \pm \text{SD}$ (%)	W_{corr} ($\text{mg cm}^{-2} \text{ h}^{-1}$)	$\eta \pm \text{SD}$ (%)	W_{corr} ($\text{mg cm}^{-2} \text{ h}^{-1}$)	$\eta \pm \text{SD}$ (%)	
Blank	-	1.358	-	1.116	1.004	-	
BS2	1.0×10^{-5}	0.377	72.2 ± 0.1	0.340	69.1 ± 0.01	0.350	65.0 ± 0.04
	1.0×10^{-4}	0.147	89.4 ± 0.5	0.108	90.3 ± 0.03	0.078	92.5 ± 0.03
	1.0×10^{-3}	0.129	90.4 ± 0.9	0.088	92.3 ± 0.05	0.036	96.2 ± 0.04
BS4	1.0×10^{-5}	0.223	83.1 ± 0.3	0.200	82.0 ± 0.60	0.186	81.1 ± 0.02
	1.0×10^{-4}	0.095	93.0 ± 0.2	0.054	95.4 ± 0.02	0.043	96.2 ± 0.04
	1.0×10^{-3}	0.045	97.2 ± 0.2	0.030	97.6 ± 0.02	0.032	97.4 ± 0.05
BS8	1.0×10^{-5}	0.261	81.6 ± 0.8	0.150	86.2 ± 0.02	0.176	82.0 ± 0.10
	1.0×10^{-4}	0.088	93.2 ± 0.2	0.042	96.1 ± 0.06	0.043	96.1 ± 0.06
	1.0×10^{-3}	0.038	97.1 ± 0.1	0.023	98.2 ± 0.04	0.020	98.3 ± 0.09

SD: standard deviation.

The table shows the increase of inhibition effectiveness with increasing immersion times for all the compounds studied in this work. This effect may be due to better interactions among the compounds in the metallic superfcies. A maximum efficiency of 98% was observed with BS8 at $1.0 \times 10^{-3} \text{ mol L}^{-1}$ concentration, corroborating with the electrochemical analysis, from which inhibitory efficiencies were obtained as 98%, 97% and 97% from EIS, LPR and PP, respectively.

3.6.2. Effect of Temperature

The temperature effect is very important in terms of observing the behavior of compounds to comprehend the mode of adsorption—i.e., by chemical or physical interactions. The weight loss experiments were performed at 303, 313, 323 and 333 K temperatures on BS2, BS4 and BS8 using the concentration that showed better efficiency ($1.0 \times 10^{-3} \text{ mol L}^{-1}$), as

noted in the electrochemical tests. Table 7 shows the data obtained in the measurements with temperature variations.

Table 7. Weight loss results for carbon steel in a HCl solution with and without BS2, BS4 and BS8 at 30, 40, 50 and 60 °C.

Inhibitor (1.0×10^{-3} mol L $^{-1}$)	30 °C		40 °C		50 °C		60 °C	
	W_{corr} (mg cm $^{-2}$ h $^{-1}$)	$\eta \pm \text{SD}$ (%)	W_{corr} (mg cm $^{-2}$ h $^{-1}$)	$\eta \pm \text{SD}$ (%)	W_{corr} (mg cm $^{-2}$ h $^{-1}$)	$\eta \pm \text{SD}$ (%)	W_{corr} (mg cm $^{-2}$ h $^{-1}$)	$\eta \pm \text{SD}$ (%)
Blank	1.358	-	2.285	-	3.485	-	4.942	-
BS2	0.121	90.1 \pm 0.10	0.228	90.2 \pm 0.30	0.361	89.3 \pm 0.05	0.647	87.2 \pm 0.08
BS4	0.045	97.4 \pm 0.20	0.091	96.3 \pm 0.1	0.187	95.4 \pm 0.10	0.360	93.4 \pm 0.10
BS8	0.038	97.2 \pm 0.10	0.080	96.0 \pm 0.04	0.150	96.1 \pm 0.10	0.310	94.2 \pm 0.05

SD: standard deviation.

Table 7 shows the anticorrosion efficiencies obtained after submitting the compounds at different temperatures, and the enhancement in the efficiencies with that of the temperature for all the compounds can be noted, suggesting interactions between the *bis*-Schiff bases and metal by chemical adsorption [54,55].

The thermodynamic parameters are very important in terms of understanding the different efficiency values obtained after the measurements. The results of the assays with temperature variations were used to construct the plot of $\ln W_{\text{corr}}$ versus $1/T$, as shown in Figure 13, which shows straight lines in the presence and absence of BS2, BS4 and BS8. The slope and intercept were calculated using the Arrhenius equation (Equation (23)).

$$\ln W_{\text{corr}} = -\frac{E_a}{RT} + \ln A \quad (23)$$

where W_{corr} = corrosion rate, T = absolute temperature, R = molar constant of gases, E_a = apparent activation energy and A = frequency factor.

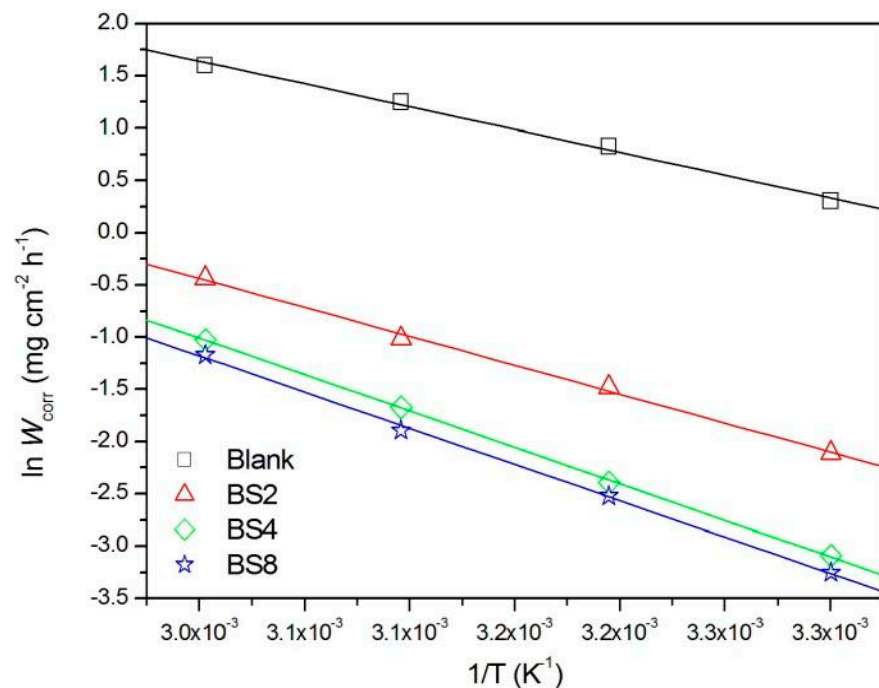


Figure 13. Arrhenius plots for carbon steel in a HCl solution (1.0 mol L^{-1}) in the lack and presence of BS2, BS4 and BS8.

Thermodynamic data, ΔH^\ddagger and ΔS^\ddagger , were determined in accordance with the Eyring equation (Equation (24)), and the E_a , ΔH^\ddagger and ΔS^\ddagger values in the lack and presence of the inhibitors are displayed in Table 8.

$$\ln \frac{W_{\text{corr}}}{T} = \ln \left[\frac{K_B}{h} e^{\frac{\Delta S^\ddagger}{R}} \right] - \frac{\Delta H^\ddagger}{RT} \quad (24)$$

where W_{corr} = corrosion rate, h = Plank constant, K_B = Boltzmann constant, ΔH^\ddagger = apparent transition activation enthalpy and ΔS^\ddagger = apparent transition activation entropy.

Table 8. Activation energy, enthalpy and entropy associated with the corrosion activity of carbon steel in a HCl solution (1.0 mol L^{-1}) with and without BS2, BS4 and BS8.

Inhibitor ($1.0 \times 10^{-3} \text{ mol L}^{-1}$)	E_a (kJ mol^{-1})	ΔH^\ddagger (kJ mol^{-1})	ΔS^\ddagger ($\text{J K}^{-1} \text{ mol}^{-1}$)
Blank	36.13	33.45	−252.96
BS2	46.08	43.80	−239.13
BS4	58.03	55.32	−209.38
BS8	57.50	54.99	−211.77

Table 8 shows the enlargement in E_a and ΔH^\ddagger values with the addition of the *bis*-Schiff bases, indicating the increase in terms of the energy barrier to start the corrosive process. All barriers were larger than that of the Blank, suggesting inhibition (lower rate) of corrosion. However, the E_a and ΔH^\ddagger values of BS4 and BS8 showed slightly inverted values due to their inhibition efficiency being equal or similar with increasing temperatures in the mass loss tests. The higher values of ΔS^\ddagger (less negatives), when compared to that of the Blank, were observed in all compounds. This can be interpreted as being due to the fact that molecules experience more degrees of freedom in a solution than on a surface, which causes a decrease in entropy. In addition, the Blank offers the greatest decrease in entropy, as the number of adsorbed water molecules is greater. Upon addition of the compounds, the quantity of water molecules that migrate to the superficies is smaller and the more voluminous the inhibitor, the greater (less negative) the activation entropy. Therefore, the trend of Blank $\Delta S^\ddagger < \text{BS2} < \text{BS8} \sim \text{BS4}$ is observed [12,45].

3.7. Scanning Electron Microscopy (SEM)

The superficies corrosion morphology for AISI 1020 carbon steel coupons was investigated using SEM in a HCl solution (1.0 mol L^{-1}) without (Blank) and with BS2, BS4 and BS8 in $1.0 \times 10^{-3} \text{ mol L}^{-1}$ after submersion for 24 h. Figure 14a shows the metallic surface before immersion. Figure 14b shows the sample immersed in a HCl solution without the compounds, where a roughness and an irregular surface can be observed, which is a consequence of metal damage due to sanding. Figure 14c–e shows a more homogeneous surface similar to that of the polished surface before immersion (Figure 14a) that corroborates the inhibitory action of the *bis*-Schiff bases.

3.8. Theoretical Studies

3.8.1. Molecular Properties of BS2, BS4 and BS8

The optimized geometries for (a) BS2, (b) BS4 and (c) BS8 (Figure 15) were obtained through density functional theory (DFT) calculations using the B3LYP/def2-QZVP computational level to understand the corrosion inhibitions of those molecules. The molecules showed total energies of $-5.549621551033 \times 10^5 \text{ kcal/mol}$ (BS2), $-6.042919424806 \times 10^5 \text{ kcal/mol}$ (BS4) and $-7.0294342323975 \times 10^5$ (BS8), respectively, at the B3LYP/def2-QZVP level of theory. The optimized structures of the compounds are not linear, as noted in Figure 15, and the aromatic rings are displaced in parallel planes separated by the aliphatic chain of sp^3 -carbons. The calculated frontier molecular orbitals for each molecule are shown in Figure 16. The frontier molecular orbitals of all molecules exhibit

similar characteristics, with the HOMO and LUMO orbitals predominantly spread across the dual aromatic rings and the double bonds linking sp^2 -carbons and the nitrogen atoms.

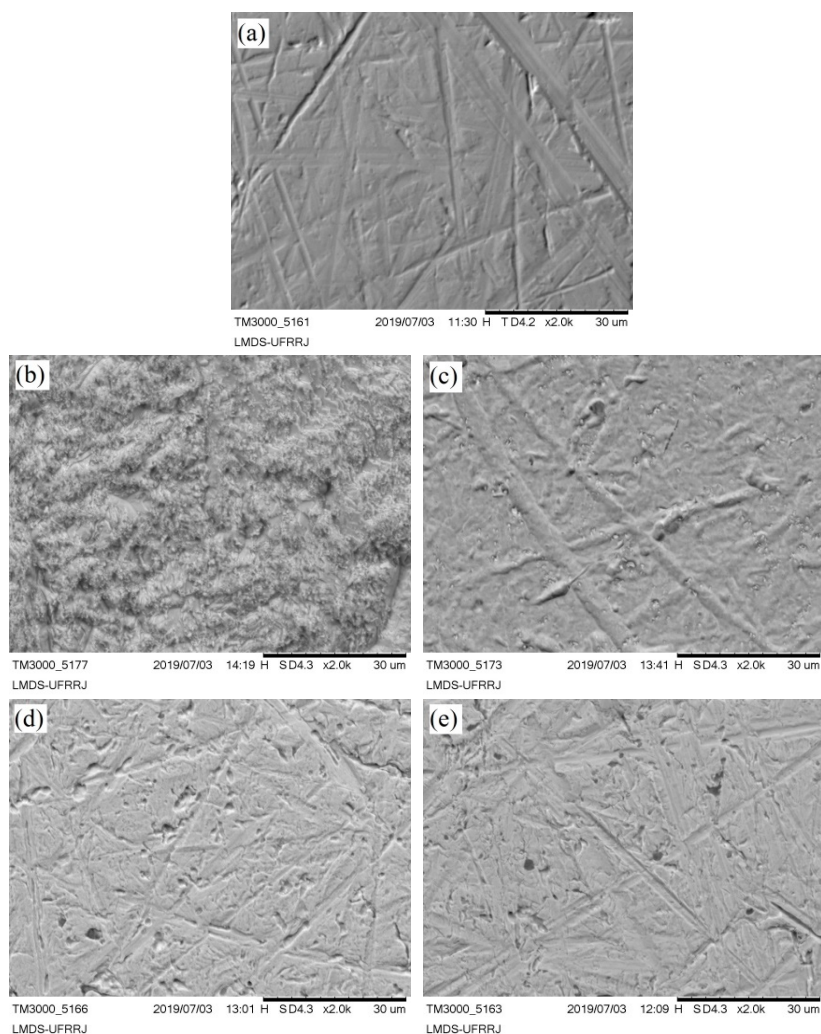


Figure 14. SEM micrograph (2000 \times) of carbon steel: (a) polished before submersion, (b) after immersion in the absence of compounds for 24 h in an acidic solution, (c) in the presence of BS2, (d) BS4 and (e) BS8 (all compounds in concentration of $1.0 \times 10^{-3} \text{ mol L}^{-1}$).

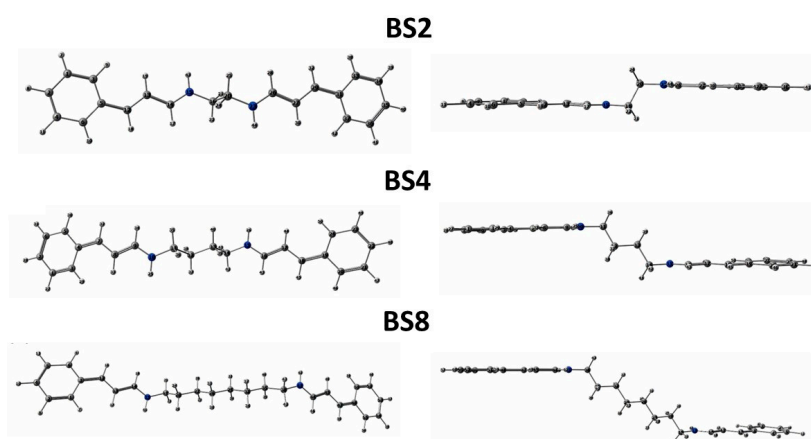


Figure 15. Optimized geometries of BS2, BS4 and BS8 obtained at the B3LYP/def2-QZVP level of theory.

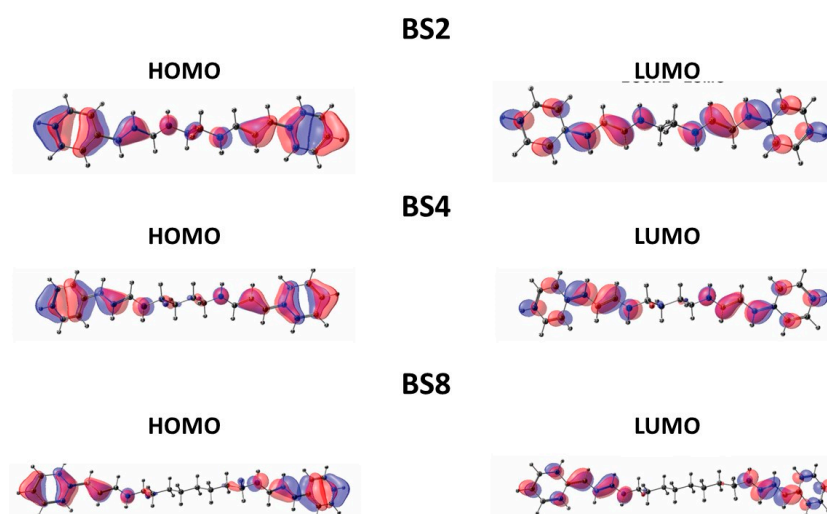


Figure 16. Frontier orbitals of BS2, BS4 and BS8 obtained at the B3LYP/def2-QZVP level of theory.

The results for the calculated reactivity molecular descriptors are shown in Table 9. The binding of an inhibitor molecule to a metal surface typically takes place in accordance with the donor–acceptor interaction [56]. Consequently, two molecular orbitals that play a crucial role in determining chemical reactivity [57] are the highest occupied molecular orbital (HOMO) and the lowest non-occupied molecular orbital (LUMO). A higher value of the HOMO orbital energy (E_{HOMO}) is expected to be related to enhanced corrosion inhibition efficiency since the valence electrons are weakly bonded, and it is donated more easily. Whereas the lower value of the energy of the LUMO orbital (E_{LUMO}) is likely related to the acceptance of electronic density since the extra negative charge is more stabilized. Thus, the BS8 molecule ($E_{\text{HOMO}} = -6.9104$ eV) has the most energetic HOMO orbital and BS2 ($E_{\text{HOMO}} = -6.9596$ eV) has the lowest, and therefore these electrons are the most stabilized by the nuclear arrangement of the molecule and have less propensity to bond with the surface. The higher energy difference of the HOMO orbitals is only 0.0492 eV, and it is between BS2 and BS8. Thus, all molecules should show similar corrosion inhibition efficiency, as already revealed from experiments. In Figure 16, it is seen that for BS2, a part of the HOMO orbital is spread in the $\text{Csp}^3\text{-Csp}^3$ bond, which can induce resistance to the electron-donation efficiency of this molecule, while BS8 only has a little part of the HOMO orbital spread between the sp^3 -carbons.

Table 9. Reactivity molecular descriptors for BS2, BS4 and BS8 obtained at the B3LYP/def2-QZVP level of theory.

Reactivity Molecular Descriptor	BS2	BS4	BS8
HOMO (eV)	−6.9596	−6.9261	−6.9104
LUMO (eV)	−3.2044	−3.0325	−2.9781
Energy Gap (eV)	3.7552	3.8936	3.9323
Ionization Potential (eV)	6.9596	6.9261	6.9104
Electron Affinity (eV)	3.2044	3.0325	2.9781
Electronegativity (eV)	5.082	4.9793	4.94425
Global Hardness (eV)	1.8776	1.9468	1.96615
Global Softness (eV^{-1})	0.532595	0.513663	0.508608
Electrophilicity index (eV)	3.438795	3.183869	3.108309
Nucleophilicity index (eV^{-1})	0.2908	0.314083	0.321718
Fraction of electrons transferred	0.510758	0.51898	0.522786

The molecule with the lowest energetic LUMO orbital is expected to show the best corrosion inhibition efficiency. However, experiments showed that BS8 with the high-

est level of energy value of the LUMO orbital has the best efficiency. These molecular orbitals accommodate electronic density from back bonding that can occur between the surface and the molecule, which means that this back bonding can stabilize the complex inhibitor surface.

The large difference between the frontier molecular orbitals energies (ΔE_{gap}) implies low chemical reactivity of species, and the small value of energy differences suggests high reactivity since it is easier to take out the electrons from the HOMO orbital and transfer them to the empty d-orbitals of the metallic surface.

The energy gap shows that even with the higher value, BS8 shows better corrosion inhibition efficiency than BS2 and BS4. The difference between the energy gaps of BS2 and BS8 is 0.1771 eV, and this value is not high enough to guarantee that BS8 is less reactive than BS2, so some other factors contribute to BS8 being the best corrosion inhibitors among these compounds.

The ionization potential of BS8 ($I = 6.9104$ eV) is slightly lower than that of BS2 ($I = 6.9596$ eV), thus it is easier for the former to donate electronic density to the iron surface as compared to BS2 (and BS4). This result is well correlated to the experiment, which demonstrates that both have similar corrosion inhibition efficiencies with BS8 being slightly more efficient. BS2 and BS4 accommodate extra electronic density better than BS8 due a higher value of electron affinity. Therefore, the electron-donation capacity of BS8 seems to be more correlated to a higher corrosion inhibition efficiency than stabilization from back bonding due to the d-orbitals on the iron surface.

The bulk iron surface is considered soft as per Pearson's HSAB theory [58], which suggests that molecules with a large energy gap are less reactive and are considered "hard" molecules, whereas species with a small energy gap are expected to be more reactive and classified as "soft" molecules. Consequently, it was expected that the softer molecule would have the best interaction with the surface. BS2 is the softer molecule and BS8 is the harder, but the difference in the global softness for these species is about 0.023987 eV. The slightly higher value of softness for BS2 is not enough to overcome the electron-donation capacity of BS8.

A higher value on the electrophilicity index (ω) implies that a molecule is more susceptible to increasing its electronic density. Therefore, it can be said that the species is classified as an electrophile, and a good nucleophile character is described to lower values of ω . The opposite can be inferred from the nucleophilicity index (ϵ), in which higher values show the susceptibility of the molecule to donate electronic density, and a strong nucleophile character is defined by higher values of ϵ . According to the results of the electrophilicity index and nucleophilicity index, BS2 is the best electrophile and the worst nucleophile, whereas BS8 is the best nucleophile and the worst electrophile.

To calculate the electron transfer from the molecule to the surface, a value of 7 eV was utilized as the electronegativity for bulk iron [56]. Typically, it is assumed that the ionization potential is the same as the electron affinity for bulk iron, resulting in a global hardness value of zero ($\eta_{\text{Fe}} = 0$) [59]. Lukovits [60] proposed that if ΔN is less than 3.6, the inhibitor efficiency increases as the nucleophilic character of the organic molecule towards the iron surface increases. The compounds show very similar values of transferred electrons, which means their inhibition efficiency increases in this order: BS2 < BS4 < BS8. The fraction of electrons transferred for all molecules is less than 3.6. This result implies that the inhibition efficiency is dependent on the capacity of electron donating of the inhibitor molecule, thus BS8 should demonstrate the highest efficiency, followed by BS4 and BS2 as the worst inhibitor. This trend agrees with the available experimental data present in this work.

3.8.2. Adsorption of the BS2, BS4 and BS8 Inhibitors

Geometries corresponding to the most stable BS2, BS4 and BS8 conformers, obtained from the molecular calculations, were optimized at the PBE-D3 level using the Quantum ESPRESSO package [28], and the resulting geometries were reoptimized within the Fe(110)

slab. The arrangement of the inhibitors on the surface was selected with the objective of prioritizing interactions between the iron surface and both aromatic rings [40,61]. The stationary points reveal that the aromatic rings adopted a horizontally aligned configuration with a maximum separation of 2.25 Å between the carbon atoms in the aromatic rings and the iron surface atoms. The aliphatic chain remains distant from the surface, except in the case of BS4 adsorption where one of the nitrogen atoms forms a bond with the surface, creating a N-Fe distance of 2.09 Å (refer to Figure 17). The greatest distance between the adsorbed aromatic rings and the Fe atoms is 2.25 Å.

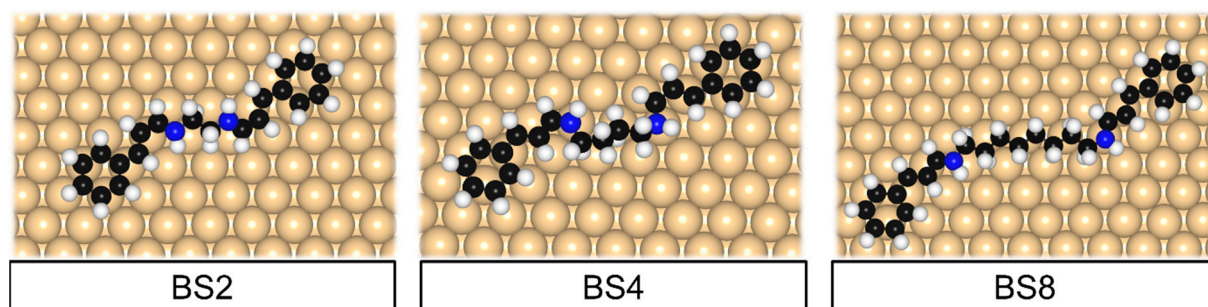


Figure 17. Adsorbed equilibrium geometries of the BS2, BS4 and BS8 on the Fe(110).

The effectiveness of the inhibitor can be associated with the elevated E_{ads} values, which are determined by the disparity in DFT energy among the corrosion inhibitor on the surface ($E_{\text{inhibitor+slab}}$), the isolated molecule ($E_{\text{gas-phase inhibitor}}$) and the bare surface (E_{slab}), as defined in Equation (25).

$$E_{\text{ads}} = E_{\text{inhibitor+slab}} - E_{\text{gas-phase inhibitor}} - E_{\text{slab}} \quad (25)$$

In this equation, $E_{\text{inhibitor+slab}}$ represents the overall energy of the compound adsorbed on the Fe(110) surface, $E_{\text{gas-phase inhibitor}}$ indicates the energy of the inhibitor in the gaseous phase, and E_{slab} corresponds to the energy of the bare surface.

The adsorption energies obtained for the BS2, BS4 and BS8 inhibitors are -1.48 , -1.80 and -4.35 eV (-34.13 , -41.51 and -100.33 kcal mol $^{-1}$), respectively. The adsorption configurations of the aromatic rings found in the inhibitors were determined based on the benzene adsorption sites, where the energetic distinction between the most favorable and less favorable adsorption modes is approximately -0.15 eV [35]. In the optimized geometries depicted in Figure 17, we can observe that the aromatic rings of BS2 and BS4 on the Fe(110) surface predominantly occupied the adsorption sites in a three-fold manner. On the other hand, the BS8 inhibitor displayed one aromatic ring in the three-fold mode, while the other ring was adsorbed at the long-bridge site.

4. Conclusions

The investigated *bis*-Schiff bases (BS2, BS4 and BS8) were synthesized in good yields in water as a solvent and microwave irradiation. All the studied inhibitors showed good corrosion inhibition effectiveness for AISI 1020 carbon steel in an acid medium of 1 mol L $^{-1}$ HCl solution. The BS8 inhibitor agent showed 98% efficiency as per the weight loss and EIS methods and 97% as per the PP and LPR tests at 1×10^{-3} mol L $^{-1}$, which should be highlighted. The adsorption of the inhibitors followed the El-Away adsorption isotherm and the modified version of the Langmuir model that indicate the capacity of compounds to interact with more sites on a metal surface due to having two imine moieties linked to phenyl rings across the aliphatic chain, which facilitates the approximation due to its degrees of freedom.

The SEM images indicated the inhibition of corrosion for carbon steel, showing that in the presence of all *bis*-Schiff bases, the metal remains as if it was not exposed to a corrosive environment.

The quantum chemical calculations demonstrated that the corrosion inhibition of the investigated compounds is controlled by the increased capacity of the compound to donate electron density to the empty d-orbitals of the iron surface. In other words, the increase of corrosion efficiency is dominated by how the molecule can act as a better nucleophile. BS8 has the HOMO orbital with more propensity to bond with the surface, so for this reason, these molecules exhibited elevated corrosion inhibitor efficiency. However, BS2 and BS4 also presented good corrosion inhibition efficiencies due to the values of the nucleophilicity index and the energy of the HOMO orbitals close to those of BS8, although they are not as good nucleophiles as BS8.

The lowest energy conformers of the BS2, BS4 and BS8 inhibitors were chosen for the study of their interactions on the surface of Fe(110). The calculated adsorption energies are -1.48 eV (-34.13 kcal mol $^{-1}$), -1.80 eV (-41.51 kcal mol $^{-1}$) and -4.35 eV (-100.33 kcal mol $^{-1}$) for BS2, BS4 and BS8, respectively, with an efficiency ranking of BS8 > BS4 > BS2, corroborating the experimental findings.

Supplementary Materials: The following supporting information can be downloaded at: <https://www.mdpi.com/article/10.3390/surfaces6040034/s1>, Figure S1: FT-IR (apt mode) spectrum of BS2; Figure S2: FT-IR (apt mode) spectrum of BS4; Figure S3: FT-IR (apt mode) spectrum of BS8; Figure S4: ^1H NMR, in chloroform, of BS2; Figure S5: ^{13}C NMR spectrum, in chloroform, of BS2; Figure S6: ^1H NMR spectrum, in chloroform, of BS4; Figure S7: ^{13}C NMR spectrum, in chloroform, of BS4; Figure S8: ^1H NMR spectrum, in chloroform, of BS8; Figure S9: ^{13}C NMR spectrum, in chloroform, of BS8.

Author Contributions: Conceptualization, P.d.L.-N., G.F.B. and A.E.; methodology, A.V., N.F.X.J., M.F.L.P.C. and F.W.Q.A.-N.; software, A.V., N.F.X.J. and F.W.Q.A.-N.; validation, A.V. and C.E.R.-S.; formal analysis, A.V., M.A.N. and G.F.B.; investigation, A.V., N.F.X.J., M.F.L.P.C. and F.W.Q.A.-N.; resources, A.E. and P.d.L.-N.; data curation, A.V.; writing—original draft preparation, A.V. N.F.X.J. and F.W.Q.A.-N.; writing—review and editing, A.E., P.d.L.-N. and G.F.B.; supervision, A.E.; project administration, A.V., C.E.R.-S. and A.E.; funding acquisition, A.E. All authors have read and agreed to the published version of the manuscript.

Funding: CNPq (Grants: 308684/2019-2) and CAPES (Finance Code 001).

Institutional Review Board Statement: Not applicable.

Informed Consent Statement: Not applicable.

Data Availability Statement: Data are contained within the article.

Acknowledgments: LNCC–SINAPAD–Santos Dumont (sdumont2019/chamada1/paper194777) and PETROBRAS (Petroleo Brasileiro S.A.).

Conflicts of Interest: The authors declare no conflict of interest.

References

1. Singh, P.; Quraishi, M.A. Corrosion inhibition of mild steel using novel bis Schiff's bases as corrosion inhibitors: Electrochemical and surface measurement. *Measurement* **2016**, *8*, 114. [[CrossRef](#)]
2. Goyal, M.; Kumar, S.; Bahadur, I.; Verma, C.; Ebenso, E.E. Organic corrosion inhibitors for industrial cleaning for ferrous and non-ferrous metals in acidic solution: A review. *J. Mol. Liq.* **2018**, *256*, 565. [[CrossRef](#)]
3. Nam, N.D.; Somers, A.; Mathesh, M.; Seter, M.; Hinton, B.; Forsyth, M.; Tan, M.Y.J. The behavior of praseodymium 4-hydroxycinnamate as an inhibitor for carbon dioxide corrosion and oxygen corrosion of steel of NaCl solutions. *Corros. Sci.* **2014**, *80*, 128. [[CrossRef](#)]
4. Quartarone, G.; Ronchin, L.; Vavasori, A.; Tortato, C.; Bonaldo, L. Inhibitive action of gramine towards corrosion of mild steel in deaerated 1.0 M in hydrochloric acid solutions. *Corros. Sci.* **2012**, *64*, 82. [[CrossRef](#)]
5. de Souza, F.S.; Spinelli, A. Caffeic acid as a green corrosion inhibitor for mild steel. *Corros. Sci.* **2009**, *51*, 642. [[CrossRef](#)]
6. Singh, D.K.; Ebenso, E.E.; Singh, M.K.; Behera, D.; Udayabhanu, G.; John, R.P. Non-toxic Schiff bases as efficient corrosion inhibitors for mild steel in 1 M HCl: Electrochemical, AFM, FE-SEM and theoretical studies. *J. Mol. Liq.* **2018**, *250*, 88. [[CrossRef](#)]
7. Arjomandi, J.; Moghanni-Bavil-Olvaei, H.; Parvin, M.H.; Lee, J.Y.; Ko, K.C.; Joshaghani, M.; Hamidian, K. Inhibition of corrosion of aluminum in alkaline solution by a novel azo-Schiff base: Experiment and theory. *J. Alloys Compd.* **2018**, *746*, 185. [[CrossRef](#)]
8. Soltani, N.; Behpour, M.; Ghoreishi, S.M.; Naeimi, H. Corrosion inhibition of mild steel in hydrochloric acid solution by some double Schiff bases. *Corros. Sci.* **2010**, *52*, 1351. [[CrossRef](#)]

9. Mallaiya, E.; Subramania, R.; Srikandan, S.S.; Gowra, S.; Rajasekaran, N.; Selvaraj, A. Electrochemical characterization of the protective film formed by the unsymmetrical Schiff's base on the mild steel surface in acid media. *Electrochim. Acta* **2011**, *56*, 3857. [CrossRef]
10. Palomar-Pardavé, M.; Romero-Romo, M.; Herrera-Hernández, H.; Abreu-Quijano, M.A.; Likhanova, N.V.; Uruchurtu, J.; Juárez-García, J.M. Influence of the alkyl chain length of 2 amino 5 alkyl 1,3,4-thiadiazole compounds on the corrosion inhibition of steel immersed in sulfuric acid solutions. *Corros. Sci.* **2012**, *54*, 231. [CrossRef]
11. Shahabi, S.; Norouzi, P.; Ganjali, M.R. Theoretical and electrochemical study of carbon steel corrosion inhibition in the presence of two synthesized Schiff base inhibitors: Application of fast Fourier transform continuous cyclic voltammetry to study the adsorption behaviour. *Int. J. Electrochem. Sci.* **2015**, *10*, 2646. Available online: <http://www.electrochemsci.org/papers/vol> (accessed on 24 March 2022). [CrossRef]
12. Liang, C.; Liu, Z.; Liang, Q.; Han, G.; Han, J.; Zhang, S.; Feng, X.Z. Synthesis of 2-aminofluorene bis Schiff base and corrosion inhibition performance for carbon steel in HCl. *J. Mol. Liq.* **2019**, *277*, 330. [CrossRef]
13. Murmu, M.; Saha, S.K.; Murmu, N.C.; Banerjee, P. Effect of stereochemical conformation into the corrosion inhibitive behaviour of double azomethine based Schiff bases on mild steel surface in 1 mol L⁻¹ HCl medium: An experimental, density functional theory and molecular dynamics simulation study. *Corros. Sci.* **2019**, *146*, 134. [CrossRef]
14. Jetti, V.; Pagadala, R.; Meshram, J.S.; Chopde, H.N.; Malladi, L. Zeolite-supported on-pot synthesis of bis-azetidiones under microwave irradiation. *J. Heterocycl. Chem.* **2013**, *50*, E160. [CrossRef]
15. Das, S.; Das, V.K.; Saikia, L.; Thakur, A.J. Environment-friendly and solvent-free synthesis of symmetrical bis-imines under microwave irradiation. *Green Chem. Lett. Rev.* **2012**, *5*, 457. [CrossRef]
16. Neese, F. The ORCA program system. *Wiley Interdiscip. Rev. Comput. Mol. Sci.* **2012**, *2*, 73. [CrossRef]
17. Becke, A.D. Density-functional thermochemistry. III. The role of exact exchange. *J. Chem. Phys.* **1993**, *98*, 5648. [CrossRef]
18. Lee, C.; Yang, W.; Parr, R.G. Development of the Colle-Salvetti correlation-energy formula into a functional of the electron density. *Phys. Rev. B* **1988**, *37*, 785. [CrossRef] [PubMed]
19. Takano, Y.; Houk, K.N. Benchmarking the conductor-like polarizable continuum model (CPCM) for aqueous solvation free energies of neutral and ionic organic molecules. *J. Chem. Theory Comput.* **2005**, *1*, 70. [CrossRef]
20. Hanwell, M.D.; Curtis, D.F.; Lonie, D.C.; Vandermeersch, C.; Zurek, E.; Hutchison, G.R. Avogadro: An advanced semantic chemical editor, visualization, and analysis platform. *J. Cheminform.* **2012**, *4*, 1. [CrossRef]
21. Chemcraft—Graphical Software for Visualization of Quantum Chemistry Computations. Available online: <https://www.chemcraftprog.com> (accessed on 14 October 2019).
22. Obot, I.B.; Macdonald, D.D.; Gasem, Z.M. Density functional theory (DFT) as a powerful tool for designing new organic corrosion inhibitors: Part 1: An overview. *Corros. Sci.* **2015**, *99*, 1. [CrossRef]
23. Fukui, K. Role of frontier orbitals in chemical reactions. *Science* **1982**, *4574*, 747. [CrossRef] [PubMed]
24. Koopmans, T. Über die zuordnung von wellenfunktionen und eigenwerten zu den einzelnen elektronen eines atoms. *Physica* **1934**, *1*, 104. [CrossRef]
25. Iczkowski, R.P.; Margrave, J.L. Electronegativity. *J. Am. Chem. Soc.* **1961**, *83*, 3547. [CrossRef]
26. Janak, J.F. Proof that $\partial E/\partial n_i = \epsilon_i$ in density-functional theory. *Phys. Rev. B* **1978**, *18*, 7165. [CrossRef]
27. von Szentpály, L. Studies on electronegativity equalization. Part 1. Consistent diatomic partial charges. *J. Mol. Struct. THEOCHEM* **1991**, *233*, 71. [CrossRef]
28. Pearson, R.G. Recent advances in the concept of hard and soft acids and bases. *J. Chem. Ed.* **1987**, *64*, 561. [CrossRef]
29. Parr, R.G.; Sventpaly, L.; Liu, S. Electrophilicity Index. *J. Am. Chem. Soc.* **1999**, *121*, 1922. [CrossRef]
30. Pearson, R.G. Hard and soft acids and bases. *J. Am. Chem. Soc.* **1963**, *85*, 3533. [CrossRef]
31. Sastri, V.S.; Perumareddi, J.R. Molecular orbital theoretical studies of some organic corrosion inhibitors. *Corrosion* **1997**, *53*, 617. [CrossRef]
32. Lukovits, I.; Kálmán, E.; Zucchi, F. Corrosion inhibitors-correlation between electronic structure and efficiency. *Corrosion* **2001**, *57*, 3. [CrossRef]
33. Perdew, J.P.; Ernzerhof, M.; Burke, K. Rationale for mixing exact exchange with density functional approximations. *J. Chem. Phys.* **1996**, *105*, 9982. [CrossRef]
34. Vanderbilt, D. Soft self-consistent pseudopotentials in a generalized eigenvalue formalism. *Phys. Rev. B* **1990**, *41*, 7892. [CrossRef] [PubMed]
35. Monkhorst, H.J.; Pack, J.D. Special points for Brillouin-zone integrations. *Phys. Rev. B* **1976**, *13*, 5188. [CrossRef]
36. Kittel, C. *Introduction to Solid State Physics*, 5th ed.; John Wiley & Sons, Inc.: New York, NY, USA, 1976.
37. Spencer, M.J.S.; Hung, A.; Snook, I.K.; Yarovsky, I. Density functional theory study of the relaxation and energy of iron surfaces. *Surf. Sci.* **2002**, *513*, 389. [CrossRef]
38. Grimme, S.; Antony, J.; Ehrlich, S.; Krieg, H. A consistent and accurate ab initio parametrization of density functional dispersion correction (DFT-D) for the 94 elements H-Pu. *J. Chem. Phys.* **2010**, *132*, 154104. [CrossRef] [PubMed]
39. Jenkins, S.J. Aromatic adsorption on metals via first-principles density functional theory. *Proc. R. Soc. A Math. Phys. Eng. Sci.* **2009**, *465*, 2949–2976. [CrossRef]

40. Liu, W.; Ruiz, V.G.; Zhang, G.X.; Santra, B.; Ren, X.; Scheffler, M.; Tkatchenko, A. Structure and energetics of benzene adsorbed on transition-metal surfaces: Density-functional theory with van der Waals interactions including collective substrate response. *New J. Phys.* **2013**, *15*, 053046. [[CrossRef](#)]
41. Makov, G.; Payne, M.C. Periodic boundary conditions in ab initio calculations. *Phys. Rev. B* **1995**, *51*, 4014. [[CrossRef](#)]
42. Mendonça, G.L.F.; Costa, S.N.; Freire, V.N.; Casciano, P.N.S.; Correia, A.N.; Lima-Neto, P. Understanding the corrosion inhibition of carbon steel and copper in sulphuric acid by amino acids using electrochemical technics allied to molecular modelling methods. *Corros. Sci.* **2017**, *115*, 41. [[CrossRef](#)]
43. Carlos, M.F.L.P.; Valbon, A.; Neves, M.A.; Santos, M.R.L.; Echevarria, A. β -Enaminoesters as novel corrosion inhibitors for carbon steel in acidic medium. *J. Braz. Chem. Soc.* **2018**, *29*, 2542. [[CrossRef](#)]
44. Valbon, A.; Neves, M.A.; Echevarria, A. Anticorrosive effect of PVP 40000 against AISI 1020 carbon steel in HCl. *Mater. Res.* **2018**, *6*, e20170847. [[CrossRef](#)]
45. Chaitra, T.K.; Mohana, K.N.S.; Tandon, H.C. Thermodynamic, electrochemical and quantum evaluation of some triazole Schiff bases as mild steel corrosion inhibitors in acid media. *J. Mol. Liq.* **2015**, *211*, 10268. [[CrossRef](#)]
46. Bredar, A.R.C.; Chown, A.L.; Burton, A.R.; Farnum, B.H. Electrochemical impedance spectroscopy of metal oxide electrodes for energy applications. *ACS Appl. Energy Mater.* **2020**, *3*, 66. [[CrossRef](#)]
47. Taylor, C.D. Corrosion informatics: An integrated approach to modelling corrosion. *Corros. Eng. Sci. Technol.* **2015**, *50*, 490. [[CrossRef](#)]
48. Kumar, C.B.P.; Mohana, K.N. Corrosion inhibitor efficiency and adsorption characteristics of some Schiff bases at mild steel/hydrochloric acid interface. *J. Taiwan Inst. Chem. Eng.* **2014**, *45*, 1031. [[CrossRef](#)]
49. Ansari, K.R.; Quraishi, M.A. Bis-Schiff bases of isatin as new and environmentally benign corrosion inhibitor for mild steel. *J. Ind. Eng. Chem.* **2014**, *20*, 2819. [[CrossRef](#)]
50. Erami, R.S.; Amirnar, M.; Meghdadi, S.; Talebian, M.; Farrokhpour, H.; Raeissi, K. Carboxamide derivatives as new corrosion inhibitors for mild steel protection in hydrochloric acid solution. *Corros. Sci.* **2019**, *151*, 190. [[CrossRef](#)]
51. Fan, B.; Ma, Y.; Wang, M.; Hao, H.; Yang, B.; Li, J.; Sun, H. Revealing the assembly mechanism of an octadecylamine based supramolecular complex on mild steel in condensate water: Correlative experimental and theoretical studies. *J. Mol. Liq.* **2019**, *292*, 111446. [[CrossRef](#)]
52. Yurt, A.; Duran, B.; Dal, H. An experimental and theoretical investigation on adsorption properties of some diphenolic Schiff bases as corrosion inhibitors at acidic solution/mild steel interface. *Arab. J. Chem.* **2014**, *7*, 732. [[CrossRef](#)]
53. Biswas, A.; Mourya, P.; Mondal, D.; Pal, S.; Udayabhanu, G. Grafting effect of gum acacia on mild steel corrosion in acidic medium: Gravimetric and electrochemical study. *J. Mol. Liq.* **2018**, *251*, 470. [[CrossRef](#)]
54. Li, X.; Deng, S.; Lin, T.; Xie, X.; Du, G. Cassava starch-sodium allylsulfonate-acryl amide graft copolymer as an effective inhibitor of aluminum corrosion in HCl solution. *J. Taiwan Inst. Chem. Eng.* **2018**, *86*, 252. [[CrossRef](#)]
55. Gerengi, H.; Mielniczek, M.; Gece, G.; Solomon, M.M. Experimental and quantum chemical evaluation of 8-hydroxyquinoline as a corrosion inhibitor for copper in 1.0 m HCl. *Ind. Eng. Chem. Res.* **2016**, *55*, 9614. [[CrossRef](#)]
56. Gong, Z.; Peng, S.; Huang, X.; Gao, L. Investigation of corrosion inhibition effect of itraconazole of copper in H₂SO₄ at different temperatures: Combining an experimental and theoretical studies. *Materials* **2018**, *11*, 2107. [[CrossRef](#)] [[PubMed](#)]
57. Ishaka, A.; Adams, F.V.; Madua, J.O.; Josepha, I.V.; Olubambi, P.A. Corrosion inhibition of mild steel in 1M hydrochloric acid using *Haematostaphis barteri* leaves extract. *Procedia Manuf.* **2019**, *35*, 1279. [[CrossRef](#)]
58. Umorena, S.A.; Solomon, M.M.; Alib, S.A.; Dafalla, H.D.M. Synthesis, characterization, and utilization of a diallylmethylamine-based cyclopolymer for corrosion mitigation in simulated acidizing environment. *Mat. Sci. Eng. C* **2019**, *100*, 897. [[CrossRef](#)]
59. Ahamad, I.; Prasad, R.; Quaraishi, M.A. Adsorption and inhibitive properties of some new Mannich bases of isatin derivatives on corrosion of mild steel in acidic media. *Corros. Sci.* **2010**, *52*, 1472. [[CrossRef](#)]
60. Chugh, B.; Singh, A.K.; Thakur, S.; Pani, B.; Pandey, A.K.; Lgaz, H.; Chung, O.M.; Ebenso, E.F. An exploration about the interaction of mild steel with hydrochloric acid in the presence of N-(benzo[d]thiazole-2-yl)-1-phenylethan-1-imines. *J. Phys. Chem. C* **2019**, *123*, 22897. [[CrossRef](#)]
61. Hensley, A.J.R.; Zhang, R.; Wang, Y.; McEwen, J.-S. Tailoring the adsorption of benzene on PdFe surfaces: A density functional theory study. *J. Phys. Chem. C* **2013**, *117*, 24317. [[CrossRef](#)]

Disclaimer/Publisher's Note: The statements, opinions and data contained in all publications are solely those of the individual author(s) and contributor(s) and not of MDPI and/or the editor(s). MDPI and/or the editor(s) disclaim responsibility for any injury to people or property resulting from any ideas, methods, instructions or products referred to in the content.